
Learning personalized treatments via IRL

Stav Belogolovsky, Philip Korsunsky, Shie Mannor, Chen Tessler and Tom Zahavy

Technion Israel Institute of Technology

{stav.belo, philip.korsunsky, tomzahavy}@gmail.com

{shie@ee, chen.tessler@campus}.technion.ac.il

*Authors contributed equally, names ordered alphabetically

Abstract

We consider the task of Inverse Reinforcement Learning in Contextual Markov Decision Processes (MDPs). In this setting, contexts that define the reward and transition kernel, are sampled from a distribution. Although the reward is a function of the context, it is not provided to the agent; instead, it observes demonstrations from an optimal policy. The goal is to learn the reward mapping so that the agent will act optimally even when encountering previously unseen contexts, also known as zero-shot transfer. We formulate this problem as a non-differential convex optimization problem and propose a novel algorithm to compute its subgradients. Based on this scheme, we analyze several methods both theoretically and empirically, where we compare both the sample complexity and scalability. Most importantly, we show both in theory and practice that our algorithms perform zero-shot transfer (generalize to new and unseen contexts). Specifically, we present empirical experiments in a dynamic treatment regime, where the goal is to learn a reward function that explains the behavior of expert physicians based on recorded data of them treating patients diagnosed with sepsis.

Many real-world sequential decision problems share three important properties — (1) *the reward function is often unknown*, yet (2) expert demonstrations can be acquired, and (3) the reward and/or dynamics often depend on a *static parameter*, also known as the context. For a concrete example, consider a dynamic treatment regime (Chakraborty & Murphy, 2014), where a clinician acts to improve a patient’s medical condition. While the patient’s dynamic measurements, e.g., heart rate and blood pressure, define the state, there are static parameters, e.g., age and weight, which determine how the patient reacts to certain treatments and what form of treatment is optimal.

The contextual model is motivated by recent trends in personalized medicine, predicted to be one of the technology breakthroughs of 2020 by MIT’s Technology Review (Juskalian et al., 2020). As opposed to traditional medicine, which provides treatment for the “average patient”, in the contextual model, patients are separated into different groups for which the medical decisions are tailored. This enables the decision-maker to provide tailored decisions (e.g., treatments) that are more effective, based on these static parameters. For instance, the correlation between the mean arterial pressure and the probability of organ injury depends on contextual features (Wesselink et al., 2018). Treating acute respiratory distress syndrome is an additional example, where the treatment goals should depend on the static patient information (the context) (Berngard et al., 2016)).

In addition to the contextual structure, we consider the setting where the reward itself is unknown to the agent. This, also, is motivated by real-world problems, in which serious issues may arise when manually attempting to define a reward signal. For instance, when treating patients with sepsis, the only available signal is the mortality of the patient at the end of the treatment (Komorowski et al., 2018). While the goal is to improve the patients’ medical condition, minimizing mortality does not necessarily capture this objective. This model is illustrated in Fig. 1. The agent observes expert interactions with the environment, either through pre-collected or interactive expert interventions.

The agent then aims to find a reward which *explains* the expert’s behavior, meaning that the expert’s policy is optimal with respect to (w.r.t.) this reward.

To tackle these problems, we propose the **Contextual Inverse Reinforcement Learning (COIRL)** framework. Similarly to Inverse Reinforcement Learning (Ng & Russell, 2000, IRL), provided expert demonstrations, the goal in COIRL is to learn a reward function that explains the expert’s behavior, i.e., a reward function for which the expert behavior is optimal. However, in COIRL, the reward is not only a function of the state features but also the context. This work aims to provide theoretical analysis and insights into this framework. As such, throughout most of the paper, we consider a linear reward (in the context and the state features). This analysis enables us to propose algorithms, analyze their behavior, and provide theoretical guarantees. We further show empirically (Section 3) that our method can be easily extended to mappings, which are non-linear in the context.

In addition to the theoretical analysis, we perform extensive testing of our methods and the relevant baselines on toy problems and on a dynamic treatment regime, which is constructed from real data. We evaluate the run-time of IRL vs. COIRL, showing that when the structure is indeed contextual, standard IRL schemes are computationally inefficient. We show that COIRL is capable of generalizing (zero-shot transfer) to unseen contexts. Simultaneously, behavioral cloning (log-likelihood action matching) is sub-optimal and struggles to find a good solution. These results show that in contextual problems, COIRL enables the agent to quickly recover a reward mapping that explains the expert’s behavior, outperforming previous methods across several metrics, and can thus be seen as a promising approach for real-life decision making.

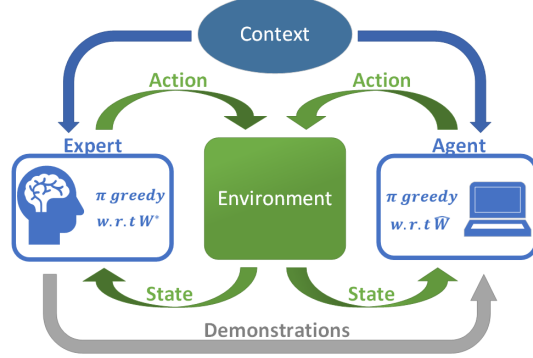


Figure 1: The COIRL framework: a context vector parametrizes the environment. For each context, the expert uses the true mapping from contexts to rewards, W^* , and provides demonstrations. The agent learns an estimation of this mapping \hat{W} and acts optimally with respect to it.

1 Preliminaries

Contextual MDPs: A Markov Decision Process (Puterman, 1994, **MDP**) is defined by the tuple $(\mathcal{S}, \mathcal{A}, P, \xi, R, \gamma)$ where \mathcal{S} is a finite state space, \mathcal{A} a finite action space, $P : \mathcal{S} \times \mathcal{S} \times \mathcal{A} \rightarrow [0, 1]$ the transition kernel, ξ the initial state distribution, $R : \mathcal{S} \rightarrow \mathbb{R}$ the reward function and $\gamma \in [0, 1]$ is the discount factor. A Contextual MDP (Hallak et al., 2015, **CMDP**) is an extension of an MDP, and is defined by $(\mathcal{C}, \mathcal{S}, \mathcal{A}, \mathcal{M}, \gamma)$ where \mathcal{C} is the context space, and \mathcal{M} is a mapping from contexts $c \in \mathcal{C}$ to MDPs: $\mathcal{M}(c) = (\mathcal{S}, \mathcal{A}, P_c, \xi, R_c, \gamma)$. For consistency with prior work, we consider the discounted infinite horizon scenario. We emphasize here that all the results in this paper can be easily extended to the episodic finite horizon and the average reward criteria. We consider a setting in which each state is associated with a feature vector $\phi : \mathcal{S} \rightarrow [0, 1]^k$, and the reward for context c is a linear combination of the state features: $R_c^*(s) = f^*(c)^T \phi(s)$. The goal is to approximate $f^*(c)$ using a function $f_W(c)$ with parameters W . This notation allows us to present our algorithms for any function approximator $f_W(c)$, and in particular a deep neural network (DNN). For the theoretical analysis, we will further assume a *linear setting*, in which the reward function and dynamics are linear in the context. Formally: $f^*(c) = c^T W^*$, $f_W(c) = c^T W$, $W^* \in \mathcal{W}$, and $P_c(s'|s, a) = \sum c_i P_i(s'|s, a)$, for some convex set \mathcal{W} . In order for the contextual dynamics to be well-defined, we assume the context space is the standard $d - 1$ dimensional simplex: $\mathcal{C} = \Delta_{d-1}$. One interpretation of this model is that each row in the mapping W^* along with the corresponding transition kernels, defines a base MDP, and the MDP for a specific context is a convex combination of these base environments.

We consider deterministic policies $\pi : \mathcal{S} \rightarrow \mathcal{A}$ which dictate the agent’s behavior at each state. The value of a policy π for context c is: $V_c^\pi = E_{\xi, P_c, \pi} [\sum_{t=0}^{\infty} \gamma^t R_c^*(s_t)] = f^*(c)^T \mu_c^\pi$, where $\mu_c^\pi := E_{\xi, P_c, \pi} [\sum_{t=0}^{\infty} \gamma^t \phi(s_t)] \in \mathbb{R}^k$ is called the *feature expectations* of π for context c . For other RL criteria there exist equivalent definitions of feature expectations; see Zahavy et al. (2020b) for the average reward. We denote by $V_c^\pi(s)$, $\mu_c^\pi(s)$ the value and feature expectations for $\xi = \mathbf{1}_s$. The Q-function is defined by: $Q_c^\pi(s, a) = R_c^*(s) + \gamma E_{s' \sim P_c(\cdot|s, a)} V_c^\pi(s')$. For the optimal policy

w.r.t. context c , we denote the above functions by V_c^*, Q_c^*, μ_c^* . For any context c , π_c^* denotes the optimal policy w.r.t. R_c^* , and $\hat{\pi}_c(W)$ denotes the optimal policy w.r.t. $\hat{R}_c(s) = f_W(c)^T \phi(s)$.

We define a ‘‘flattening’’ operator, converting a matrix to a vector: $\mathbb{R}^{d \times k} \rightarrow \mathbb{R}^{d \cdot k}$ by $\underline{W} = [w_{1,1}, \dots, w_{1,k}, \dots, w_{d,1}, \dots, w_{d,k}]$. We also define the operator \odot as the composition of the flattening operator and the outer product: $u \odot v = [u_1 v_1, \dots, u_1 v_k, \dots, u_d v_1, \dots, u_d v_k]$. Thus, the value of policy π for context c is given by $V_c^\pi = c^T W^* \mu_c^\pi = \underline{W}^{*T} (c \odot \mu_c^\pi)$, where $\|c \odot \mu_c^\pi\|_1 \leq \frac{k}{1-\gamma}$.

Learned dynamics: The majority of apprenticeship learning (AL) papers consider the problem of learning the transition kernel and initial state distribution as an orthogonal ‘supervised learning’ problem to the AL problem. Their algorithm starts by approximating the dynamics from samples and then executes the AL algorithm on the approximated dynamics (Abbeel & Ng, 2004; Syed & Schapire, 2008). In this work, we adhere to this principle. We also note that existing methods, such as Modi et al. (2018), can be used to learn a transition kernel and an initial state distribution parametrized by the context. Thus, we assume P_c is known when discussing suggested methods in Section 2.

2 Methods

Apprenticeship learning (AL) algorithms are designed to find a policy that performs as well as the expert for any reward signal. In the supplementary material (Appendix A) we provide a summary of how two of the most known algorithms, MWAL (Syed & Schapire, 2008) and the projection method (Abbeel & Ng, 2004) achieve that. In the CMDP formulation, on the other hand, the policy is a function of the context; thus, it is not clear what class of policies would suit such an analysis. Instead, we follow the approach that was taken in the CMDP literature and aim to learn the linear mapping from contexts to rewards (Hallak et al., 2015; Modi et al., 2018; Modi & Tewari, 2019). This requires us to design an IRL algorithm instead of an AL algorithm, i.e., to approximate the mapping $f^*(c)$ by observing an expert (for each context c , the expert provides a demonstration from π_c^*).

To achieve this goal, we now derive and analyze convex optimization algorithms for COIRL. We begin with Proposition 1, which introduces the objective function, here, we show that if W is a minimizer of Eq. (1), then the expert policy is optimal w.r.t. reward \hat{R}_c for any context.

Proposition 1. *Eq. (1) satisfies the following properties: (1) For any W the loss is greater or equal to zero. (2) If $\text{Loss}(W) = 0$ then for any context, the expert policy is the optimal policy w.r.t. reward $\hat{R}_c(s) = c^T W \phi(s)$ (proof is provided in the appendices).*

$$\text{Loss}(W) = \mathbb{E}_c \max_{\pi} [f_W(c) \cdot (\mu_c^\pi - \mu_c^*)] = \mathbb{E}_c [f_W(c) \cdot (\mu_c^{\hat{\pi}_c(W)} - \mu_c^*)]. \quad (1)$$

Evaluating this objective requires finding, for all contexts, both the optimal policy $\hat{\pi}_c(W)$ and its feature expectations $\mu_c^{\pi_c(W)}$. Although the feature expectations can be computed through policy evaluation (solving a set of linear equations), finding $\hat{\pi}_c(W)$ requires solving the MDP, e.g., using standard RL methods such as value or policy iteration. As finding the policy is non-trivial, Eq. (1) is non-differentiable w.r.t. W . We therefore consider two optimization schemes that do not involve differentiation: (i) subgradients and (ii) randomly perturbing the loss function (finite differences).

Although the loss is non-differentiable, Proposition 2 below shows that in the special case that $f_W(c)$ is a linear function, Eq. (1) is convex and Lipschitz continuous. Furthermore, it provides a method to compute its subgradients.

Proposition 2. *Let $f_W(c) = c^T W$ such that $\text{Loss}(W) = L_{\text{lin}}(W) = \mathbb{E}_c [c^T W \cdot (\mu_c^{\hat{\pi}_c(W)} - \mu_c^*)]$:*
(1) $L_{\text{lin}}(W)$ is a convex function. (2) $g(W) = \mathbb{E}_c [c \odot (\mu_c^{\hat{\pi}_c(W)} - \mu_c^)]$ is a subgradient of $L_{\text{lin}}(W)$. (3) L_{lin} is Lipschitz continuous with Lipschitz constant $L = \frac{2}{1-\gamma}$ w.r.t. $\|\cdot\|_\infty$ and $L = \frac{2\sqrt{dk}}{1-\gamma}$ w.r.t. $\|\cdot\|_2$.*

Note that $g(W) \in \mathbb{R}^{d \times k}$ is a matrix; we will sometimes refer to it as a matrix and sometimes as a flattened vector, depending on the situation. Finally, $g(W)$ is given in expectation over contexts and trajectories (feature expectations). We will later see how to replace $g(W)$ with an unbiased estimate, which can be computed by observing a single expert trajectory for a single context.

Proposition 2 identifies $L_{\text{lin}}(W)$ as a convex function and provides a method to compute its subgradients. A standard method for minimizing a convex function over a convex set is the

subgradient projection algorithm (Bertsekas, 1997), where the iterates are updated following $W_{t+1} = \text{Proj}_{\mathcal{W}}\{W_t - \alpha_t g(W_t)\}$, where $f(W_t)$ is a convex function, $g(W_t)$ is a subgradient of $f(W_t)$, and α_t the learning rate. \mathcal{W} is required to be a convex set; we will consider two particular cases, the ℓ_2 ball (Abbeel & Ng, 2004) and the simplex (Syed & Schapire, 2008). As scaling of the reward by a constant does not affect the resulting policy, these sets are not restricting.

Next, we consider a generalization of the subgradient projection algorithm that is called the mirror descent algorithm (Nemirovsky & Yudin, 1983, MDA): $W_{t+1} = \arg \min_{W \in \mathcal{W}} \{W \cdot \nabla f(W_t) + \frac{1}{\alpha_t} D_\psi(W, W_t)\}$, where $D_\psi(W, W_t)$ is a Bregman distance (see the supplementary material for definitions), associated with a strongly convex function ψ . In the supplementary material (Theorem 1), we restate a theorem that characterizes the convergence rate of MDA. The requirements of MDA is the selection of the norm, and a definition of the divergence ψ . In the supplementary material, we derive and analyze two specific instances for MDA (Appendix B): projected subgradient descent (PSGD) and exponential weights (EW). In addition, we consider a derivative-free algorithm for computing subgradients, based on *Evolution Strategies* (Salimans et al., 2017, ES) and analyze it.

Practical MDA: One of the ‘‘miracles’’ of MDA is its robustness to noise. If g_t is replaced with an unbiased estimate \tilde{g}_t , such that $\mathbb{E}\tilde{g}_t = g_t$ and $\mathbb{E}\|\tilde{g}_t\| \leq L$, the same convergence results (Theorem 1) still stand (Robbins & Monro, 1951) (see, for example, Bubeck (2015, Theorem 6.1)). Such an unbiased estimate can be obtained through: (i) sample a context c_t ; (ii) compute $\hat{\pi}_{c_t}(W_t)$ and its feature expectations; (iii) observe a single expert demonstration $\tau_i^E = \{s_0^i, a_0, s_1^i, a_1, \dots\}$, where a_i is chosen by $\pi_{c_t}^*$; and (iv) let $\hat{\mu}_i = \sum_{t \in [0, \dots, |\tau_i^E| - 1]} \gamma^t \phi(s_t^i)$ be the accumulated discounted features across the trajectory such that $\mathbb{E}\hat{\mu}_i = \mu_{c_t}^*$.

However, for $\hat{\mu}_i$ to be an unbiased estimate of $\mu_{c_t}^*$, τ_i^E needs to be of infinite length. Thus one can either (1) execute the expert trajectory online, and terminate it at each time step with probability $1 - \gamma$ (Kakade & Langford, 2002), or (2) execute a trajectory of length $H = \frac{1}{1-\gamma} \log(1/\epsilon_H)$. As the trajectory length is unbounded, the estimate $\hat{\mu}_i$, obtained from the first approach, cannot be shown to concentrate to $\mu_{c_t}^*$ via Hoeffding type inequalities. Nevertheless, it is possible to obtain a concentration inequality using the fact that the length of each trajectory is bounded in high probability (similar to Zahavy et al. (2020b)). The second approach can only guarantee that $\|g_t - \mathbb{E}\tilde{g}_t\| \leq \epsilon_H$ (Syed & Schapire, 2008). Hence, using the robustness of MDA to adversarial noise (Zinkevich, 2003), we get that MDA converges with an additional error of ϵ_H , i.e., $L_{\text{lin}}(\frac{1}{T} \sum_{t=1}^T W_t) - L_{\text{lin}}(W^*) \leq \mathcal{O}(\frac{1}{\sqrt{T}}) + \epsilon_H$. While this sampling mechanism has the cost of a controlled bias, usually, it is more practical, in particular when using offline data.

Algorithm 1 MDA for COIRL

Input: a norm $\|\cdot\|$, a strongly convex function ψ with strong convexity parameter σ w.r.t. the norm, a convex set \mathcal{W} with diameter D w.r.t. the norm, L a Lipschitz constant, T number of iterations
Initialize $W_1 \in \mathcal{W}$
for $t = 1, \dots, T$ **do**
 Observe c, μ_c^*
 Compute $\hat{\pi}_c(W_t), \mu_c^{\hat{\pi}_c(W_t)}$
 Compute $g_t = c \odot (\mu_c^{\hat{\pi}_c(W_t)} - \mu_c^*)$
 Set learning rate $\alpha_t = \frac{D}{L} \sqrt{\frac{2\sigma}{t}}$
 $W_{t+1} = \arg \min_{W \in \mathcal{W}} \{W \cdot g_t + \frac{1}{\alpha_t} D_\psi(W, W_t)\}$
end for
return $\frac{1}{T} \sum_{t=1}^T W_t$

2.1 Existing approaches

Next, we compare the MDA algorithm with existing baselines. We focus on methods that can be used for zero-shot generalization across contexts or tasks. Hence, we omit the discussion of ‘‘meta inverse reinforcement learning’’ methods, which focus on few-shot generalization (Xu et al., 2018). Our focus is on three approaches: (1) standard IRL methods applied to a model which incorporates the context as part of the state, (2) behavioral cloning (BC) (Pomerleau, 1989) with contextual policies, and (3) the ellipsoid method for IRL (Amin et al., 2017) which we extend to the contextual setting.

Application of IRL to COIRL problems: We first examine the approach of incorporating the context into the state, by defining $\mathcal{S}' = \mathcal{C} \times \mathcal{S}$, and applying IRL methods to this environment which captures all contexts. This construction limits the context space to a finite one, as opposed to COIRL, which works trivially with an infinite context space. At first glance, this method results in the same scalability and sample complexity as COIRL; however, when considering the inner loop in which an

Table 1: Summary of theoretical guarantees.

		Scalability		Sample Complexity		Extension to DNNs
		Deterministic	Stochastic	Deterministic	Stochastic	
MDA	PSGD	$\mathcal{O}(dk)$		$\mathcal{O}(1/\epsilon^2)$	$\mathcal{O}(1/\epsilon^2)$	✓
	EW	$\mathcal{O}(\log dk)$				✗
	ES	$\mathcal{O}(dk)$	$\mathcal{O}(d^2k^2)$	$\mathcal{O}(\log(1/\epsilon))$		✓
	Ellipsoid	$\mathcal{O}(d^2k^2)$	$\mathcal{O}(d^2k^4)$			✗

optimal policy is calculated, COIRL has the advantage of smaller state space by a factor of $|\mathcal{C}|$. This results in significantly better run-time for large context spaces. Our experiments in the supplementary material evaluate the run-time of this approach, compared to COIRL, for increasingly large context spaces. These results demonstrate that the run-time of IRL scales with $|\mathcal{C}|$ while COIRL is unaffected by $|\mathcal{C}|$, making COIRL much more practical for environments with many or infinite contexts.

In addition, we consider Transition Regularized Imitation Learning (TRIL), a model-free approach for learning the expert policy (Lee et al., 2019). TRIL does not distinguish between the context and state and considers them as a large MDP which is solved with a DRL approach. The idea is to train a DNN to predict feature expectations of policies, from off policy data, which is then used for AL.

Contextual policies: Behavioral Cloning (BC) is another option for learning contextual policies – policies that are functions of both state and context $\pi(c, s)$, through supervised learning, without learning the reward function. While BC saw some successful applications (Ratliff et al., 2007), it has a fundamental flaw; the learned policy affects the distribution of states it encounters, causing a covariate shift in test-time, leading to compounding errors (Ross & Bagnell, 2010). In Section 3.2, we show empirically that BC generalizes poorly until much of the expert policy is observed.

The ellipsoid method: Finally, we consider the ellipsoid method for IRL (Amin et al., 2017). While previously discussed methods learn from offline data, the ellipsoid is an online method that relies on expert oversight during test-time. Here, the agent suggests a policy for each new context, which is then evaluated by the expert. If the policy is near-optimal, the agent executes it. Otherwise, the expert intervenes and provides its feature expectations to the agent for training. The ellipsoid method maintains an ellipsoid-shaped feasibility set, which is reduced with each provided demonstration. As this is impractical, Amin et al. (2017) analyze a framework that relaxes these requirements. In this relaxation, the expert evaluates the Q-value of individual actions that the agent suggests. If a suggested action is sub-optimal, the expert provides a trajectory from that point to the agent.

While the expert supervision guarantees a certain level of performance, it limits the applicability of this method. In addition, in the relaxed framework, this method’s scalability and sample complexity do not surpass our COIRL methods (Table 1). In the supplementary material, we provide a formal explanation of this method and how it applies to COIRL, as well as proofs for the upper bounds on the number of demonstrations required. We compare the ellipsoid method to COIRL methods in the online framework and show that it does not perform as well in terms of generalization and regret.

3 Experiments

We divide this Section into two sub-sections. We begin with experiments in two simulated environments, a grid world, and the autonomous driving simulation (Abbeel & Ng, 2004). These are fairly small domains, so they allow us to test all the methods and eliminate those that are inefficient. The second Section focuses on the dynamic treatment regime. We begin with a simulation, where the expert trajectories are generated from the optimal policy for each context. Finally, we apply the methods that performed best in simulation to real-world data and evaluate the action-matching of the methods using real clinician observations. Our code is provided in github.com/coirl/coirl_code.

3.1 Small domains

Grid world. In this experiment, we compare a contextual version of the projection algorithm for AL (Abbeel & Ng, 2004) with PSGD (COIRL). The projection algorithm is applied to a large MDP, where the state space includes both the contexts and the states, as described in the previous Section. We considered a wide range of grid worlds and measured each algorithm’s performance for

different sized context spaces. While both algorithms were able to find the optimal policy, it takes the projection algorithm more time to achieve this goal (Fig. 7 in the appendices). At the same time, the run-time of PSGD is not affected by the number of contexts. These results are summarized in Fig. 2(c), suggesting that AL in a large MDP does not scale with the number of contexts.

Autonomous driving simulation. This domain simulates a three-lane highway (Fig. 8 in the appendices) with two visible cars (A and B). The agent, controlling car A, can drive both on the highway and off-road. Car B drives in a fixed lane, at a slower speed than car A. When car B leaves the frame, it is replaced by a new car, which appears in a random lane at the top of the screen. The state features denote the speed of car A, whether it is on the road and whether it has collided with car B. The context implies different priorities for the agent; should it prefer speed or safety? Is going off-road a valid option? The mapping from the contexts to the true reward induces different behaviors for different contexts, making generalization a challenging task.

We begin with a comparison between the COIRL methods and the ellipsoid method in the **ellipsoid setting**. Here, the agent’s policy is evaluated by an expert for every new context revealed. An expert demonstration will be provided only if its value is not ϵ -close to the optimal policy value. Thus, the amount of given demonstrations is equal to the number of times that the agent is not ϵ -close to the optimal policy value, which measures how much intervention is required by an external expert. We would expect a ‘good’ method to be ϵ -optimal for most revealed contexts, and therefore it should observe a small number of demonstrations. In Fig. 2(a), we present the accumulated amount of expert demonstrations given at each time-step, and in Fig. 2(b), the value of the agent on a holdout test set (after each demonstration). The results suggest that all the methods eventually reach the expert’s value; however, the descent methods are more sample efficient than the ellipsoid method and require fewer expert demonstrations. In addition, the ellipsoid method demands constant expert monitoring, which might not be available in real-world problems.

Next, we compare the descent methods in an **online setting**. Each descent step is performed on a context- μ pair. The context is sampled uniformly from the simplex, and μ is the feature expectation of a policy optimal for this context. For each method, we measure the normalized value of the proposed policies w.r.t. the real reward, the loss (Eq. (1)), and the accuracy, measured as the percentage of hit, which represents how often the expert and agent policies match. These criteria are evaluated on a holdout set of contexts, unseen during training. The x-axis corresponds to the number of contexts seen during training, i.e., the number of subgradient steps taken.

The goal of the MDA algorithms for COIRL is to find a mapping $W \in \mathcal{W}$, where \mathcal{W} is a ball in $\|\cdot\|_2$ for PSGD and ES and the simplex for EW (more details in Appendix B). Thus, in order to compare the three methods, we set \mathcal{W} to be the simplex (which is a subset of the $\|\cdot\|_2$ ball) in this experiment.

Inspecting Fig. 3 we can see that all the MDA algorithms find the optimal mappings. We also observe a strong correlation between ‘loss minimization’ and ‘value maximization’. The EW method converges the fastest as the theoretical results suggest (Section 2). Relying on the uncertainty set being the simplex gives it an advantage, but limits its applicability to problems where the uncertainty set should not be the simplex (e.g. the mapping may have negative weights). It is also harder to

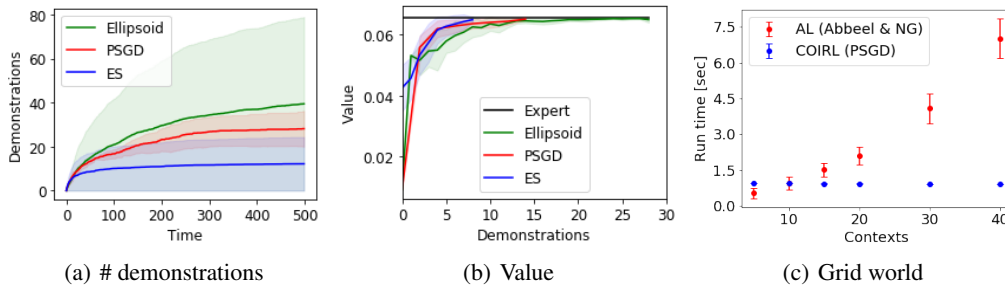


Figure 2: Simulations in the Autonomous driving and a Grid world domains. **Fig. 2(a) and Fig. 2(b):** compare the ellipsoid, ES and PSGD methods in the autonomous driving simulation. Fig. 2(a) present the number of demonstrations requested by each method as a function of time, and Fig. 2(b) presents performance. **Fig. 2(c):** time to convergence in grid worlds of varying context-space size.

extend this approach to work with neural networks. ES also performs better than PSGD but requires extensive computations. This requirement makes the ES method computationally expensive and prevents it from scaling to larger environments. For that reasons, and despite the fact that PSGD is slightly less sample efficient, we focus on PSGD in the next experiments.

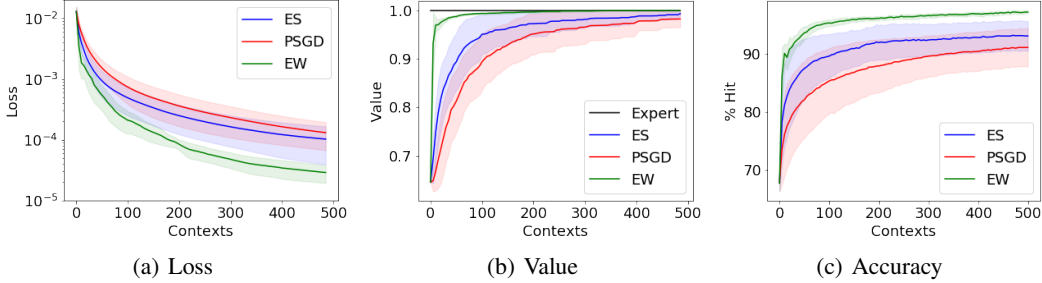


Figure 3: **Online learning curve in the autonomous driving simulation.** We compare the loss, value and accuracy, where the accuracy is relative to the expert’s behavior. As can be seen, all descent methods minimize the loss and achieve high value. Additionally, we observe that while they do attain relatively high accuracy, they find policies which are optimal yet differ from the experts.

3.2 Sepsis treatment

From here on, we focus on the main application of this paper, a decision-making process for treating patients with sepsis. We use the MIMIC-III data set (Johnson et al., 2016), which is composed of hospital electronic databases, social security, and archives from critical care information systems, acquired during routine hospital care. We begin with a sepsis treatment simulator, which we built from this data set, and follow the data processing steps taken in Jeter et al. (2019) to extract the relevant data in the form of normalized measurements of sepsis patients during their hospital admission and the treatments that were given to each patient. The measurements include dynamic measures, e.g., heart rate, blood pressure, body temperature, blood analysis standard measures (glucose, platelets count, etc.), as well as static measures such as age, gender, and more.

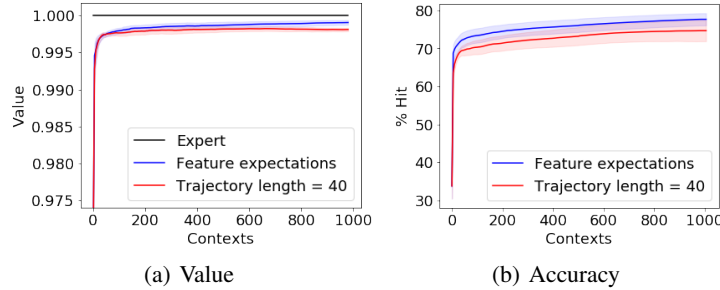


Figure 4: **Online setting in sepsis treatment.** We compare the relative value and accuracy when the agent is provided the feature expectations or finite length trajectories. We observe that while as the feature expectations are more informative, the performance is slightly better. However, notice that the difference is negligible and amounts to less than 0.5% difference in the relative value.

We construct a CMDP from the data, in which a clinician acts to improve a sick patient’s medical condition. The context represents patient features that are constant during treatment, such as age and height. The state summarizes dynamic measurements of the patient, e.g., blood pressure and EEG readouts. The actions represent different combinations of fluids and vasopressors, drugs commonly provided to restore and maintain blood pressure in sepsis patients. The mapping from the context to the true reward is constructed from the data. In these simulations, the expert trajectories were generated from the optimal policy (for a given context) w.r.t. the true context-reward mapping.

In the **online** setting, we evaluate the PSGD method in two setups. (1) when the expert’s feature expectations for each context are given, and (2) When only a single expert demonstration is given for each patient (practical MDA). We observe in Fig. 4 that PSGD performs better when given feature expectations, as expected. An important observation is that high accuracy is not necessary for high value, as our agents achieve near-perfect value with relatively low accuracy. This reinforces the use of IRL for imitation learning tasks, as it supports the claim that the reward function, not the policy, is the most concise and accurate representation of task (Abbeel & Ng, 2004). In the **offline setting**, we evaluate COIRL and contextual BC (Section 2.1). We test their ability to generalize with a limited amount of data. The motivation for this experiment comes from real-life applications, where the data available is often limited in size. The data, similarly to the online setting, is constructed from context-trajectory pairs. In this setting, we minimize the loss function (Eq. (1)) by taking descent steps on mini-batches sampled from the data set. Each method’s performance is evaluated as a function of the train-set size (the amount of context-trajectory pairs used for training). We consider a non-linear mapping from context to reward, hence we use a DNN estimator (described in the supplementary).

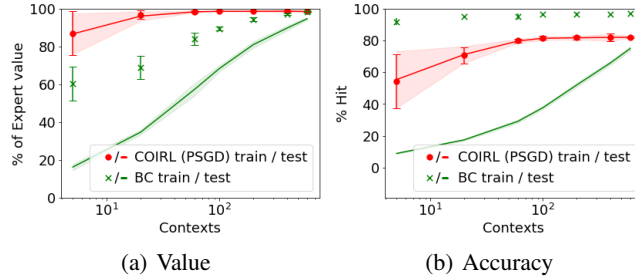


Figure 5: **Offline setting in sepsis treatment: non-linear mapping.** The x-axis denotes the number of contexts in the training set (logarithmic scale). Results on the train data are represented using circles and x’s, and the results on a holdout test data-set are represented as lines. COIRL generalizes well for a small amount of train data, where the performance on the train data and on the test data is similar. Contextual BC performance on the train set is almost perfect, but requires a large amount of demonstrations in order to attain good performance on the test set.

Fig. 5 presents the performance of COIRL and contextual BC, when provided with a fixed amount of data. The results show that in the sepsis treatment domain, COIRL can generalize well for a small amount of training data compared to contextual BC, for both value and accuracy. As expected, although BC is able to fit the train data (high accuracy on the train set), as it solves the wrong objective, COIRL performs better in terms of achieved value (on both the train and test contexts).

Real-world. So far we presented results on simulated variations of the environment to test the properties of COIRL, taking a sequence of steps to make the simulations more realistic. Finally, we focus on the real-world data. Since the true mapping is no longer known, we can only measure the accuracy of our resulted policies. We observed that while accuracy does not necessarily imply value (i.e., many policies can attain optimal value), these measures are often correlated. In addition, since the MDP’s true dynamics are now unknown, we estimate them from the data itself.

Data processing: We follow the steps done in Komorowski et al. (2018) to construct time-series data of static and dynamic measurements. The data is divided into trajectories, where each trajectory represents a different patient. We consider only trajectories of length greater than 10 that represent 40 hours. The processed data consists of 14, 591 trajectories, divided into a 60-20-20 train-validation-test partition. Each trajectory corresponds to a static measurement vector and a time series of dynamic measurement vectors, with time steps of 4 hours. In the following experiments, each model is trained over the train set, until an early stopping criteria is met on the validation set. We then report the accuracy (action matching with the clinician’s actions) on the holdout test set. **Model fitting:** The contexts and the states constructed from static and dynamic measurements, respectively. In our model, the contexts are in \mathbb{R}^7 and include the gender, age, weight, GCS, elixhauser co-morbidity score, whether the patient was mechanically ventilated at s_0 and whether the patient has been re-admitted to the hospital. The actions are defined to be the number of vasopressors given to a patient at each time slot, and five discrete actions are constructed by dividing the possible values into five bins. The state space is constructed by clustering the observed patient dynamic measurements from the data with

K-means (MacQueen et al., 1967). The clustering process is repeated for different numbers of states and different measurements, guided by clinicians. The chosen model consists 5000 states that were clustered by mean blood pressure, diastolic blood pressure, shock index, cumulative balance of fluids, and the fluids given to a patient. We consider context-dependent dynamics; the contexts are clustered into five clusters, and the dynamics for each cluster are then estimated using the train data.

Methods: For COIRL we report results for the *linear* and the *non-linear* mappings; for both, we use a discount factor $\gamma = 0.7$. The *non-linear* setup uses a DNN to learn the mapping between the context and the reward. For BC we also use a DNN, as we found it to work much better than a linear model. We experimented with different sets of features as inputs and chose the features that we found to give the best performance. The DNN architectures are described in the supplementary material. Each method was trained and evaluated over five seeds. The results, Table 2, show that COIRL with a non-linear mapping attains the best performance, while the linear mapping achieves poor accuracy. BC performs well overall, but not as good as COIRL. In Lee et al. (2019), the authors use a similar data set and action space. Their best results achieved by TRIL, attain a lower hit-rate than COIRL and with higher variance. These results suggest that the contextual hypothesis better represents the real world, i.e., that physicians indeed provide personalized treatments.

Method		Accuracy %
COIRL	Non-linear	83.74 ± 1.02
	Linear	45.17 ± 7.14
BC		73.12 ± 0.82
TRIL		80 ± 2

Table 2: Test accuracy of various methods with real-world data. COIRL (with non-linear mapping) achieves the highest accuracy.

4 Discussion

Motivated by current trends in personalized medicine (Juskalian et al., 2020), we proposed the Contextual Inverse Reinforcement Learning framework and formulated it as a convex optimization problem. Since the objective is not differentiable, we proposed two schemes based on subgradient descent (MDA and ES) and two cutting plane methods (Ellipsoid). Given an offline data set of expert treatments, these algorithms are shown to find near-optimal treatment policies for patients (MDPs) that were not included in the training set (zero-shot transfer). We analyzed the convergence properties of each algorithm and summarized the results in Table 1. In the future, we plan to extend our approach to cope with infinitely large MDPs and non-linear mappings by combining COIRL with meta-learning (Finn et al., 2017), so we can learn new policies for new contexts faster.

We performed an extensive empirical evaluation of the proposed algorithms and compared them to existing baselines. Our results suggest that the ellipsoid schemes perform sub-optimally compared to the other methods, as the theory suggests. We also compared our approach to a contextual deep behavioral cloning baseline. It was not clear how to define the policy class for this algorithm, so we did not analyze it theoretically. Empirically, we found it to be a strong baseline, but COIRL outperformed it. Previous work (Abbeel & Ng, 2004) explain this by the fact that while the reward/value is smooth (Lipschitz) w.r.t. the context, the policy is not. As a small change in the context may lead to a large switch in the policy (the optimal actions change in certain states), we observe that BC struggles. This can also be seen in the fact that COIRL often reaches imperfect action-matching (accuracy) yet attains the optimal return. COIRL achieved the highest accuracy in the challenging task of predicting the clinicians’ treatment in the real world sepsis treatment data set, outperforming existing DRL baselines (Gottesman et al., 2019). This suggests that sepsis treatment can be modeled as a contextual MDP; we hope that these findings will motivate future work in using contextual MDPs to model real-world decision making.

References

- Abbeel, P. and Ng, A. Y. Apprenticeship learning via inverse reinforcement learning. In *Proceedings of the twenty-first international conference on Machine learning*, pp. 1. ACM, 2004.
- Amin, K., Jiang, N., and Singh, S. Repeated inverse reinforcement learning. In *Advances in Neural Information Processing Systems*, pp. 1815–1824, 2017.
- Beck, A. and Teboulle, M. Mirror descent and nonlinear projected subgradient methods for convex optimization. *Operations Research Letters*, 31:167–175, 2003.
- Berngard, S. C., Beitler, J. R., and Malhotra, A. Personalizing mechanical ventilation for acute respiratory distress syndrome. *Journal of thoracic disease*, 8(3):E172, 2016.
- Bertsekas, D. P. Nonlinear programming. *Journal of the Operational Research Society*, 48(3): 334–334, 1997.
- Boyd, S. P. and Barratt, C. H. *Linear controller design: limits of performance*. Prentice Hall Englewood Cliffs, NJ, 1991.
- Bubeck, S. Convex optimization: Algorithms and complexity. *Foundations and Trends® in Machine Learning*, 8(3-4):231–357, 2015.
- Chakraborty, B. and Murphy, S. A. Dynamic treatment regimes. *Annual review of statistics and its application*, 1:447–464, 2014.
- Finn, C., Abbeel, P., and Levine, S. Model-agnostic meta-learning for fast adaptation of deep networks. In *Proceedings of the 34th International Conference on Machine Learning-Volume 70*, pp. 1126–1135. JMLR. org, 2017.
- Garber, D. and Hazan, E. A linearly convergent variant of the conditional gradient algorithm under strong convexity, with applications to online and stochastic optimization. *SIAM Journal on Optimization*, 26(3):1493–1528, 2016.
- Gottesman, O., Johansson, F., Komorowski, M., Faisal, A., Sontag, D., Doshi-Velez, F., and Celi, L. A. Guidelines for reinforcement learning in healthcare. *Nature medicine*, 25(1):16–18, 2019.
- Hallak, A., Di Castro, D., and Mannor, S. Contextual markov decision processes. *arXiv preprint arXiv:1502.02259*, 2015.
- Hazan, E. Introduction to online convex optimization. *Foundations and Trends® in Optimization*, 2 (3-4):157–325, 2016.
- Jaggi, M. Revisiting frank-wolfe: Projection-free sparse convex optimization. 2013.
- Jeter, R., Josef, C., Shashikumar, S., and Nemati, S. Does the "artificial intelligence clinician" learn optimal treatment strategies for sepsis in intensive care?, 2019. URL <https://github.com/point85AI/Policy-Iteration-AI-Clinician.git>.
- Johnson, A. E., Pollard, T. J., Shen, L., Lehman, L.-w. H., Feng, M., Ghassemi, M., Moody, B., Szolovits, P., Anthony Celi, L., and Mark, R. G. Mimic-iii, a freely accessible critical care database. *Scientific Data*, 3:160035, May 2016. ISSN 2052-4463. doi: 10.1038/sdata.2016.35. URL <http://dx.doi.org/10.1038/sdata.2016.35>.
- Juskalian, R., Regalado, A., Orcutt, M., Piore, A., Rotman, D., Patel, N. V., Lichfield, G., Hao, K., Chen, A., and Temple, J. Mit technology review, February 2020. URL <https://www.technologyreview.com/lists/technologies/2020/>.
- Kakade, S. and Langford, J. Approximately optimal approximate reinforcement learning. In *International conference on Machine learning*, pp. 267–274, 2002.
- Komorowski, M., Celi, L. A., Badawi, O., Gordon, A. C., and Faisal, A. A. The artificial intelligence clinician learns optimal treatment strategies for sepsis in intensive care. *Nature Medicine*, 24(11): 1716, 2018.

- Lee, D., Srinivasan, S., and Doshi-Velez, F. Truly batch apprenticeship learning with deep successor features. *arXiv preprint arXiv:1903.10077*, 2019.
- MacQueen, J. et al. Some methods for classification and analysis of multivariate observations. In *Proceedings of the fifth Berkeley symposium on mathematical statistics and probability*, pp. 281–297. Oakland, CA, USA, 1967.
- Modi, A. and Tewari, A. Contextual markov decision processes using generalized linear models. *arXiv preprint arXiv:1903.06187*, 2019.
- Modi, A., Jiang, N., Singh, S., and Tewari, A. Markov decision processes with continuous side information. In *Algorithmic Learning Theory*, pp. 597–618, 2018.
- Nemirovsky, A. S. and Yudin, D. B. In *Problem complexity and method efficiency in optimization*. Wiley, New York, 1983.
- Nesterov, Y. and Spokoiny, V. Random gradient-free minimization of convex functions. *Foundations of Computational Mathematics*, 17(2):527–566, 2017.
- Ng, A. Y. and Russell, S. J. Algorithms for inverse reinforcement learning. In *Icml*, volume 1, pp. 2, 2000.
- Pomerleau, D. A. Alvin: An autonomous land vehicle in a neural network. In *Advances in neural information processing systems*, pp. 305–313, 1989.
- Puterman, M. L. *Markov decision processes: discrete stochastic dynamic programming*. John Wiley & Sons, 1994.
- Ratliff, N., Bagnell, J. A., and Srinivasa, S. S. Imitation learning for locomotion and manipulation. In *2007 7th IEEE-RAS International Conference on Humanoid Robots*, pp. 392–397. IEEE, 2007.
- Robbins, H. and Monroe, S. A stochastic approximation method. *The annals of mathematical statistics*, pp. 400–407, 1951.
- Ross, S. and Bagnell, D. Efficient reductions for imitation learning. In *Proceedings of the thirteenth international conference on artificial intelligence and statistics*, pp. 661–668, 2010.
- Salimans, T., Ho, J., Chen, X., Sidor, S., and Sutskever, I. Evolution strategies as a scalable alternative to reinforcement learning. *arXiv preprint arXiv:1703.03864*, 2017.
- Syed, U. and Schapire, R. E. A game-theoretic approach to apprenticeship learning. In *Advances in neural information processing systems*, pp. 1449–1456, 2008.
- Wesselink, E., Kappen, T., Torn, H., Slooter, A., and van Klei, W. Intraoperative hypotension and the risk of postoperative adverse outcomes: a systematic review. *British journal of anaesthesia*, 2018.
- Xu, K., Ratner, E., Dragan, A., Levine, S., and Finn, C. Learning a prior over intent via meta-inverse reinforcement learning. *arXiv preprint arXiv:1805.12573*, 2018.
- Zahavy, T., Cohen, A., Kaplan, H., and Mansour, Y. Apprenticeship learning via frank-wolfe. 2020a.
- Zahavy, T., Cohen, A., Kaplan, H., and Mansour, Y. Average reward reinforcement learning with unknown mixing times. *Proceedings of the Thirty-Sixth Conference on Uncertainty in Artificial Intelligence*, 2020b.
- Zinkevich, M. Online convex programming and generalized infinitesimal gradient ascent. In *Proceedings of the 20th International Conference on Machine Learning (ICML-03)*, pp. 928–936, 2003.

Appendices

A Background on Apprenticeship Learning and Inverse Reinforcement Learning

In Apprenticeship Learning (AL), the reward function is unknown, and we denote the MDP without the reward function (also commonly called a controlled Markov chain) by $\text{MDP}\backslash R$. Similarly, we denote a CMDP without a mapping of context to reward by $\text{CMDP}\backslash M$.

Instead of manually tweaking the reward to produce the desired behavior, the idea is to observe and mimic an expert. The literature on IRL is quite vast and dates back to (Ng & Russell, 2000; Abbeel & Ng, 2004). In this setting, the reward function (while unknown to the apprentice) equals to a linear combination of a set of known features, as we defined above. The expert demonstrates a set of trajectories that are used to estimate the feature expectations of its policy π_E , denoted by μ_E . The goal is to find a policy π , whose feature expectations are close to this estimate, and hence will have a similar return with respect to any weight vector w .

Formally, AL is posed as a two-player zero-sum game, where the objective is to find a policy π that does at least as well as the expert with respect to any reward function of the form $r(s) = w \cdot \phi(s)$, $w \in \mathcal{W}$. That is we solve

$$\max_{\pi \in \Pi} \min_{w \in \mathcal{W}} [w \cdot \mu(\pi) - w \cdot \mu_E] \quad (2)$$

They define the problem of approximately solving Eq. (2) as AL, i.e., finding π such that

$$\forall w \in \mathcal{W} : w \cdot \mu(\pi) \geq w \cdot \mu_E - \epsilon + f^*. \quad (3)$$

If we denote the value of Eq. (2) by f^* then, due to the von-Neumann minimax theorem we also have that

$$f^* = \min_{w \in \mathcal{W}} \max_{\pi \in \Pi} [w \cdot \mu(\pi) - w \cdot \mu_E]. \quad (4)$$

We will later use this formulation to define the IRL objective, i.e., finding $w \in \mathcal{W}$ such that

$$\forall \pi \in \Pi : w \cdot \mu_E \geq w \cdot \mu(\pi) - \epsilon - f^*; \quad (5)$$

Abbeel & Ng (2004) suggested two algorithms to solve Eq. (3) for the case that \mathcal{W} is a ball in the euclidean norm; one that is based on a maximum margin solver and a simpler projection algorithm. The latter starts with an arbitrary policy π_0 and computes its feature expectation μ_0 . At step t they define a reward function using weight vector $w_t = \mu_E - \bar{\mu}_{t-1}$ and find the policy π_t that maximizes it. $\bar{\mu}_t$ is a convex combination of feature expectations of previous (deterministic) policies $\bar{\mu}_t = \sum_{j=1}^t \alpha_j \mu(\pi_j)$. They show that in order to get that $\|\bar{\mu}_T - \mu\| \leq \epsilon$, it suffices to run the algorithm for $T = O(\frac{k}{(1-\gamma)^2 \epsilon^2} \log(\frac{k}{(1-\gamma)\epsilon}))$ iterations.

Recently, Zahavy et al. (2020a) showed that the projection algorithm is, in fact, equivalent to a Frank-Wolfe method for finding the projection of the feature expectations of the expert on the feature expectations polytope – the convex hull of the feature expectations of all the deterministic policies in the MDP. The Frank-Wolfe analysis gives the projection method of Abbeel & Ng (2004) a slightly tighter bound of $T = O(\frac{k}{(1-\gamma)^2 \epsilon^2})$. In addition, a variation of the FW method that is based on taking “away steps” (Garber & Hazan, 2016; Jaggi, 2013) achieves a linear rate of convergence, i.e., it is logarithmic in ϵ .

Another type of algorithms, based on online convex optimization, was proposed by Syed & Schapire (2008). In this approach, in each round the “reward player” plays an online convex optimization algorithm on losses $l_t(w_t) = w_t \cdot (\mu_E - \mu(\pi_t))$; and the “policy player” plays the best response, i.e., the policy π_t that maximizes the return $\mu(\pi_t) \cdot w_t$ at time t . The results in (Syed & Schapire, 2008) use a specific instance of MDA where the optimization set is the simplex and distances are measured w.r.t. $\|\cdot\|_1$. This version of MDA is known as multiplicative weights or Hedge. The algorithm runs for T steps and returns a mixed policy ψ that draws with probability $1/T$ a policy π_t , $t = 1, \dots, T$.

Thus,

$$\begin{aligned} f^* &\leq \frac{1}{T} \sum_{t=1}^T \max_{\pi \in \Pi} [w_t \cdot \mu(\pi) - w_t \cdot \mu_E] \\ &= \frac{1}{T} \sum_{t=1}^T [w_t \cdot \mu(\pi_t) - w_t \cdot \mu_E] \end{aligned} \quad (6)$$

$$\leq \min_{w \in \mathcal{W}} \frac{1}{T} \sum_{t=1}^T w \cdot [\mu(\pi_t) - \mu_E] + O\left(\frac{\sqrt{\log(k)}}{(1-\gamma)\sqrt{T}}\right) \quad (7)$$

$$= \min_{w \in \mathcal{W}} w \cdot (\mu(\psi) - \mu) + O\left(\frac{\sqrt{\log(k)}}{(1-\gamma)\sqrt{T}}\right), \quad (8)$$

where Eq. (6) follows from the fact that the policy player plays the best response, that is, π_t is the optimal policy w.r.t. the reward w_t ; Eq. (7) follows from the fact that the reward player plays a no-regret algorithm, e.g., online MDA. Thus, they get that $\forall w \in \mathcal{W} : w \cdot \mu(\psi) \geq w \cdot \mu + f^* - O\left(\frac{1}{\sqrt{T}}\right)$.

1

B MDA instances for COIRL

In this section we restate a result on the convergence rate of MDA and provide two MDA instances. We then provide details on a derivative free method called evolutionary strategies and restate its convergence guarantess in the convex case.

Theorem 1 (Convergence rate of MDA). *Let ψ be a σ -strongly convex function on \mathcal{W} w.r.t. $\|\cdot\|$, and let $D^2 = \sup_{W_1, W_2 \in \mathcal{W}} D_\psi(W_1, W_2)$. Let f be convex and L -Lipschitz continuous w.r.t. $\|\cdot\|$. Then, MDA with $\alpha_t = \frac{D}{L} \sqrt{\frac{2\sigma}{t}}$ satisfies: $f(\frac{1}{T} \sum_{t=1}^T W_t) - f(W^*) \leq DL \sqrt{\frac{2}{\sigma T}}$.*

We refer the reader to Beck & Teboulle (2003) and Bubeck (2015) for the proof.

Projected subgradient descent (PSGD): Let \mathcal{W} be an ℓ_2 ball with radius 1. Fix $\|\cdot\|_2$, and $\psi(W) = \frac{1}{2} \|W\|_2^2$. ψ is strongly convex w.r.t. $\|\cdot\|_2$ with $\sigma = 1$. The associated Bregman divergence is given by $D_\psi(W_1, W_2) = 0.5 \|W_1 - W_2\|_2^2$. Thus, mirror descent is equivalent to PSGD. $D^2 = \max_{W_1, W_2 \in \mathcal{W}} D_\psi(W_1, W_2) \leq 1$, and according to Proposition 2, $L = \frac{2\sqrt{dk}}{1-\gamma}$. Thus, we have that the learning rate is $\alpha_t = (1-\gamma)\sqrt{\frac{1}{2dk t}}$ and the update to W is given by

$$\tilde{W} = W_t - \alpha_t g_t, \quad W_{t+1} = \tilde{W} / \|\tilde{W}\|_2,$$

and according to Theorem 1 we have that after T iterations,

$$L_{\text{lin}}\left(\frac{1}{T} \sum_{t=1}^T W_t\right) - L_{\text{lin}}(W^*) \leq \mathcal{O}\left(\frac{\sqrt{dk}}{(1-\gamma)\sqrt{T}}\right).$$

Exponential Weights (EW): Let \mathcal{W} be the standard $dk-1$ dimensional simplex. Let $\psi(W) = \sum_i W(i) \log(W(i))$. ψ is strongly convex w.r.t. $\|\cdot\|_1$ with $\sigma = 1$. We get that the associated Bregman divergence is given by

$$D_\psi(W_1, W_2) = \sum_i W_1(i) \log\left(\frac{W_1(i)}{W_2(i)}\right),$$

also known as the Kullback-Leibler divergence. In addition,

$$D^2 = \max_{W_1, W_2 \in \mathcal{W}} D_\psi(W_1, W_2) \leq \log(dk)$$

and according to Proposition 2, $L = \frac{2}{1-\gamma}$. Thus, we have that the learning rate is $\alpha_t = (1-\gamma)\sqrt{\frac{\log(dk)}{2t}}$. Furthermore, the projection onto the simplex w.r.t. this distance amounts to a simple

¹The O notation hides the dependency in k and γ .

renormalization $W \leftarrow W/\|W\|_1$. Thus, we get that MDA is equivalent to the exponential weights algorithm and the update to w is given by

$$\forall i \in [1..dk], \tilde{W}(i) = W_t(i) \exp(-\alpha_t g_t(i)), \quad W_{t+1} = \tilde{W}/\|\tilde{W}\|_1.$$

Finally, according to Theorem 1 we have that after T iterations,

$$L_{\text{lin}}\left(\frac{1}{T} \sum_{t=1}^T W_t\right) - L_{\text{lin}}(W^*) \leq \mathcal{O}\left(\frac{\sqrt{\log(dk)}}{(1-\gamma)\sqrt{T}}\right).$$

Evolution strategies for COIRL.

We also consider a derivative-free algorithm for computing subgradients, based on *Evolution Strategies* (Salimans et al., 2017, ES). For convex optimization problems, ES is a gradient-free descent method based on computing finite differences (Nesterov & Spokoiny, 2017). The subgradient in ES is computed by sampling random perturbations and computing the loss for them, in the following form

For $j=1, \dots, m$ do
 Sample $u_j \sim \mathcal{N}(0, \rho^2) \in \mathcal{R}^{dk}$,
 $g^j = \text{Loss}\left(W_t + \frac{\nu u_j}{\|u_j\|}\right) \frac{\nu u_j}{\|u_j\|}$,
End For,

and the subgradient is given by

$$g_t = \frac{1}{m\rho} \sum_{j=1}^m g^j. \quad (9)$$

Theorem 2 presents the sample complexity of PSGD with the subgradient in Eq. (9) for the case that the loss is convex, as in L_{lin} . While this method has looser upper-bound guarantees compared to MDA (Theorem 1), Nesterov & Spokoiny (2017) observed that in practice, it often outperforms subgradient-based methods. Thus, we test ES empirically and compare it with the subgradient method (Section 2). Additionally, Salimans et al. (2017) have shown the ability of ES to cope with high dimensional non-convex tasks (DNNs).

Theorem 2 (ES Convergence Rate (Nesterov & Spokoiny, 2017)). *Let $L_{\text{lin}}(W)$ be a non-smooth convex function with Lipschitz constant L , such that $\|W_0 - W^*\| \leq D$, step size of $\alpha_t = \frac{D}{(dk+4)\sqrt{T+1}L}$ and $\nu \leq \frac{\epsilon}{2L\sqrt{dk}}$ then in $T = \frac{4(dk+4)^2 D^2 L^2}{\epsilon^2}$ ES finds a solution which is bounded by $\mathbb{E}_{U_{T-1}}[L_{\text{lin}}(\hat{W}_T)] - L_{\text{lin}}(W^*) \leq \epsilon$, where $U_T = \{u_0, \dots, u_T\}$ denotes the random variables of the algorithm up to time T and $\hat{W}_T = \arg \min_{t=1, \dots, T} L_{\text{lin}}(W_t)$.*

C Proofs for Section 2

Definition 1 (Bregman distance). *Let $\psi : \mathcal{W} \rightarrow \mathbb{R}$ be strongly convex and continuously differential in the interior of \mathcal{W} . The Bregman distance is defined by $D_\psi(x, y) = \psi(x) - \psi(y) - (x - y) \cdot \nabla \psi(y)$, where ψ is strongly convex with parameter σ .*

Definition 2 (Conjugate function). *The conjugate of a function $\psi(y)$, denoted by $\psi^*(y)$ is*

$$\max_{x \in \mathcal{W}} \{x \cdot y - \psi(x)\}.$$

Example: let $\|\cdot\|$ be a norm on \mathbb{R}^n . The associated dual norm, denoted $\|\cdot\|_*$, is defined as $\|z\|_* = \sup\{z^\top x \mid \|x\| \leq 1\}$. The dual norm of $\|\cdot\|_2$ is $\|\cdot\|_2$, and the dual norm of $\|\cdot\|_1$ is $\|\cdot\|_\infty$. Before we begin with the proof of Proposition 2, we make the following observation. By definition, $\hat{\pi}_c(W)$ is the optimal policy w.r.t. $c^T W$; i.e., for any policy π we have that

$$c^T W \cdot \mu_{\hat{\pi}_c(W)}^{\hat{\pi}_c(W)} \geq c^T W \cdot \mu_c^\pi. \quad (10)$$

Proof of Proposition 1.

Fix W . For any context c , we have that $\mu(\hat{\pi}_c)$ is the optimal policy w.r.t. reward $f_W(c)$, thus, $f_W(c) \cdot (\mu(\hat{\pi}_c(W)) - \mu(\pi_c^*)) \geq 0$. Therefore we get that $\text{Loss}(W) \geq 0$. For W^* , we have that $\mu(\hat{\pi}_c(W)) = \mu(\pi_c^*)$, thus $\text{Loss}(W^*) = 0$.

For the second statement, note that $\text{Loss}(W) = 0$ implies that $\forall c, f_W(c) \cdot (\mu(\hat{\pi}_c(W)) - \mu(\pi_c^*)) = 0$. This can happen in one of two cases. (1) $\mu(\hat{\pi}_c(W)) = \mu(\pi_c^*)$, in this case $\pi_c^*, \hat{\pi}_c(W)$ have the same feature expectations. Therefore, they are equivalent in terms of value. (2) $\mu(\hat{\pi}_c(W)) \neq \mu(\pi_c^*)$, but $f_W(c) \cdot (\mu(\hat{\pi}_c(W)) - \mu(\pi_c^*)) = 0$. In this case, $\pi_c^*, \hat{\pi}_c(W)$ have different feature expectations, but still achieve the same value w.r.t. reward $f_W(c)$. Since $\hat{\pi}_c(W)$ is an optimal policy w.r.t. this reward, so is π_c^* . \square

Proof of Proposition 2.

1. We need to show that $\forall W_1, W_2 \in \mathcal{W}, \forall \lambda \in [0, 1]$, we have that

$$\begin{aligned} L_{\text{lin}}(\lambda W_1 + (1 - \lambda)W_2) &\leq \lambda L_{\text{lin}}(W_1) + (1 - \lambda)L_{\text{lin}}(W_2) \\ L_{\text{lin}}(\lambda W_1 + (1 - \lambda)W_2) &= \mathbb{E}_c \left[c^T (\lambda W_1 + (1 - \lambda)W_2) \cdot \left(\mu_c^{\hat{\pi}_c(\lambda W_1 + (1 - \lambda)W_2)} - \mu_c^* \right) \right] \\ &= \lambda \mathbb{E}_c \left[c^T W_1 \cdot \left(\mu_c^{\hat{\pi}_c(\lambda W_1 + (1 - \lambda)W_2)} - \mu_c^* \right) \right] \\ &\quad + (1 - \lambda) \mathbb{E}_c \left[c^T W_2 \cdot \left(\mu_c^{\hat{\pi}_c(\lambda W_1 + (1 - \lambda)W_2)} - \mu_c^* \right) \right] \\ &\leq \lambda \mathbb{E}_c \left[c^T W_1 \cdot \left(\mu_c^{\hat{\pi}_c(W_1)} - \mu_c^* \right) \right] + (1 - \lambda) \mathbb{E}_c \left[c^T W_2 \cdot \left(\mu_c^{\hat{\pi}_c(W_2)} - \mu_c^* \right) \right] \\ &= \lambda L_{\text{lin}}(W_1) + (1 - \lambda)L_{\text{lin}}(W_2), \end{aligned}$$

where the inequality follows from Eq. (10).

2. Fix $z \in \mathcal{W}$. We have that

$$\begin{aligned} L_{\text{lin}}(z) &= \mathbb{E}_c \left[c^T z \cdot \left(\mu_c^{\hat{\pi}_c(z)} - \mu_c^* \right) \right] \\ &\geq \mathbb{E}_c \left[c^T z \cdot \left(\mu_c^{\hat{\pi}_c(W)} - \mu_c^* \right) \right] \\ &= L_{\text{lin}}(W) + (z - W) \cdot \mathbb{E}_c \left[c \odot \left(\mu_c^{\hat{\pi}_c(W)} - \mu_c^* \right) \right], \end{aligned}$$

where the inequality follows from Eq. (10).

3. Recall that a bound on the dual norm of the subgradients implies Lipschitz continuity for convex functions. Thus it is enough to show that $\forall W \in \mathcal{W}, \|g(W)\|_p = \|\mathbb{E}_c [c \odot (\mu_c^{\hat{\pi}_c(W)} - \mu_c^*)]\|_p \leq L$. Let $p = \infty$, we have that

$$\begin{aligned} \|g(W)\|_\infty &= \left\| \mathbb{E}_c c \odot \left(\mu_c^{\hat{\pi}_c(W)} - \mu_c^* \right) \right\|_\infty \\ &\leq \mathbb{E}_c \|c \odot \left(\mu_c^{\hat{\pi}_c(W)} - \mu_c^* \right)\|_\infty \quad (\text{Jensen inequality}) \\ &\leq \mathbb{E}_c \|c\|_\infty \|\mu_c^{\pi_i} - \mu_c^{\pi_j}\|_\infty \leq \frac{2}{1 - \gamma}. \end{aligned} \tag{11}$$

where in Eq. (11) we used the fact that $\forall \pi$ we have that $\|\mu_c^\pi\|_\infty \leq \frac{1}{1 - \gamma}$, thus, for any π_i, π_j ,

$$\|\mu_c^{\pi_i} - \mu_c^{\pi_j}\|_\infty \leq \frac{2}{1 - \gamma}.$$

Therefore, $L = \frac{2}{1 - \gamma}$ w.r.t. $\|\cdot\|_\infty$. Since $\|\cdot\|_2 \leq \sqrt{dk} \|\cdot\|_\infty$ we get that $L = \frac{2\sqrt{dk}}{1 - \gamma}$ w.r.t. $\|\cdot\|_2$. \square

D Ellipsoid algorithms for COIRL

In this section we present the ellipsoid method, introduced to the IRL setting by Amin et al. (2017). We extend this method to the contextual setting, and focus on finding a linear mapping $W \in \mathcal{W}$ where $\mathcal{W} = \{W : \|W\|_\infty \leq 1\}$, and $W^* \in \mathcal{W}$.

The algorithm maintains an ellipsoid-shaped feasibility set that contains W^* . Formally, for a vector u that defines the center of the ellipsoid, and an invertible matrix Q , an ellipsoid is defined by $\{x : (x - u)Q^{-1}(x - u) \leq 1\}$. At every step, the current estimation W_t of W^* is defined as the center of the ellipsoid, and the agent acts optimally w.r.t. this estimation (Appendix D, top left). If the agent performs sub-optimally, the expert provides a demonstration in the form of its feature expectations for c_t : $\mu_{c_t}^*$. The feature expectations are used to generate a linear constraint (hyperplane) on the ellipsoid that is crossing its center (Appendix D, top right). Under this constraint, we construct a new feasibility set that is half of the previous ellipsoid and still contains W^* (Appendix D, bottom right). For the algorithm to proceed, we compute a new ellipsoid that is the minimum volume enclosing ellipsoid (MVEE) around this “half-ellipsoid” (Appendix D, bottom left). These updates are guaranteed to gradually reduce the volume of the ellipsoid, as shown in Lemma 1, until its center is a mapping which induces ϵ -optimal policies.

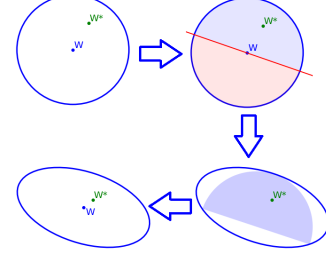


Figure 6: The ellipsoid algorithm proceeds in an iterative way, using linear constraints to gradually reduce the size of the ellipsoid until the center defines an ϵ -optimal solution.

Lemma 1 (Boyd & Barratt (1991)). *If $B \subseteq \mathbb{R}^D$ is an ellipsoid with center w , and $x \in \mathbb{R}^D \setminus \{0\}$, we define $B^+ = \text{MVEE}(\{\theta \in B : (\theta - w)^T x \geq 0\})$, then: $\frac{\text{Vol}(B^+)}{\text{Vol}(B)} \leq e^{-\frac{1}{2(D+1)}}$.*

Theorem 3 below shows that this algorithm achieves a polynomial upper bound on the number of sub-optimal time-steps. The proof is adapted from (Amin et al., 2017) to the contextual setup.

Algorithm 2 Ellipsoid algorithm for COIRL

Initialize: $\Theta_0 \leftarrow B_\infty(0, 1) = \{x \in \mathbb{R}^{d \times k} : \|x\|_\infty \leq 1\}$

$\Theta_1 \leftarrow \text{MVEE}(\Theta_0) : \underline{W}_1 = 0, Q_1 = dkI$

for $t = 1, 2, \dots$ **do**

Observe c_t , let \underline{W}_t be the center of Θ_t

Play episode using $\hat{\pi}_t = \arg \max_{\pi} c_t^T W_t \mu_{c_t}^\pi$

if $V_{c_t}^* - V_{c_t}^{\hat{\pi}_t} > \epsilon$ **then**

$\mu_{c_t}^*$ is revealed

Let $a_t = c_t \odot (\mu_{c_t}^* - \mu_{c_t}^{\hat{\pi}_t})$

$\Theta_{t+1} \leftarrow \text{MVEE}(\{\theta \in \Theta_t : \theta^T a_t \geq \underline{W}_t^T a_t\})$

else

$\Theta_{t+1} \leftarrow \Theta_t$

end if

end for

MVEE($\{\theta \in \Theta_t : \theta^T a_t \geq \underline{W}_t^T a_t\}$):

$$\tilde{a}_t = \frac{-1}{\sqrt{a_t^T Q_t a_t}} a_t$$

$$\underline{W}_{t+1} = \underline{W}_t - \frac{1}{dk+1} Q_t \tilde{a}_t$$

$$Q_{t+1} = \frac{d^2 k^2}{d^2 k^2 - 1} (Q_t - \frac{2}{dk+1} Q_t \tilde{a}_t \tilde{a}_t^T Q_t)$$

Theorem 3. *In the linear setting where $R_c^*(s) = c^T W^* \phi(s)$, for an agent acting according to Algorithm 1, the number of rounds in which the agent is not ϵ -optimal is $\mathcal{O}(d^2 k^2 \log(\frac{dk}{(1-\gamma)\epsilon}))$.*

Remark 1. *Note that the ellipsoid method presents a new learning framework, where demonstrations are only provided when the agent performs sub-optimally. Thus, the theoretical results in this section cannot be directly compared with those of the descent methods. We further discuss this in Appendix E.2.*

Remark 2. The ellipsoid method does not require a distribution over contexts - an adversary may choose them. MDA can also be easily extended to the adversarial setting via known regret bounds on online MDA (Hazan, 2016).

Practical ellipsoid algorithm: In many real-world scenarios, the expert cannot evaluate the value of the agent’s policy and cannot provide its policy or feature expectations. To address these issues, we follow Amin et al. (2017) and consider a relaxed approach, in which the expert evaluates each of the individual actions performed by the agent rather than its policy, and provides finite roll-outs instead of a policy or feature expectations (Algorithm 3). We define the expert criterion for providing a demonstration to be $Q_{c_t}^*(s, a) + \epsilon < V_{c_t}^*(s)$ for each state-action pair (s, a) in the agent’s trajectory.

Near-optimal experts: In addition, we relax the optimality requirement of the expert and instead assume that, for each context c_t , the expert acts optimally w.r.t. W_t^* which is close to W^* ; the expert also evaluates the agent w.r.t. this mapping. This allows the agent to learn from different experts, and from non-stationary experts whose judgment and performance slightly vary over time. If a sub-optimal action w.r.t. W_t^* is played at state s , the expert provides a roll-out of H steps from s to the agent. As this roll-out is a sample of the optimal policy w.r.t. W_t^* , we aggregate n examples to assure that with high probability, the linear constraint that we use in the ellipsoid algorithm does not exclude W^* from the feasibility set. Note that these batches may be constructed across different contexts, different experts, and different states from which the demonstrations start. Theorem 4 below upper bounds the number of sub-optimal actions that Algorithm 3 chooses.²

Theorem 4. For an agent acting according to Algorithm 3, $H = \lceil \frac{1}{1-\gamma} \log(\frac{8k}{(1-\gamma)\epsilon}) \rceil$ and $n = \lceil \frac{512k^2}{(1-\gamma)^2\epsilon^2} \log(4dk(dk+1) \log(\frac{16k\sqrt{dk}}{(1-\gamma)\epsilon})/\delta) \rceil$, with probability of at least $1 - \delta$, if $\forall t : \underline{W}_t^* \in B_\infty(\underline{W}^*, \frac{(1-\gamma)\epsilon}{8k}) \cap \Theta_0$ the number of rounds in which a sub-optimal action is played is $\mathcal{O}\left(\frac{d^2k^4}{(1-\gamma)^2\epsilon^2} \log\left(\frac{dk}{(1-\gamma)\delta\epsilon} \log\left(\frac{dk}{(1-\gamma)\epsilon}\right)\right)\right)$.

Algorithm 3 Batch ellipsoid algorithm for COIRL

Initialize: $\Theta_0 \leftarrow B_\infty(0, 1) = \{x \in \mathbb{R}^{d \cdot k} : \|x\|_\infty \leq 1\}$
 $\Theta_1 \leftarrow \text{MVEE}(\Theta_0)$
 $i \leftarrow 0, \bar{Z} \leftarrow 0, \bar{Z}^* \leftarrow 0$
for $t = 1, 2, 3, \dots$ **do**
 c_t is revealed, Let \underline{W}_t be the center of Θ_t
Play episode using $\hat{\pi}_t = \arg \max_\pi c_t^T W_t \mu_{c_t}^\pi$
 $\Theta_{t+1} \leftarrow \Theta_t$
if a sub-optimal action a is played at state s **then**
Expert provides H -step trajectory $(s_0^E = s, s_1^E, \dots, s_H^E)$. Let $\hat{x}_i^{*,H}$ be the H -step sample of the expert’s feature expectations for $\xi_i' = \mathbf{1}_s$: $\hat{x}_i^{*,H} = \sum_{h=0}^H \gamma^h \phi(s_h^E)$
Let x_i be the agent’s feature expectations for $\xi_i' : E_{\xi_i', P_{c_t}, \pi_t}[\sum_{h=0}^\infty \gamma^h \phi(s_h)]$
Denote $z_i = c_t \odot x_i, \hat{z}_i^{*,H} = c_t \odot \hat{x}_i^{*,H}$
 $i \leftarrow i + 1, \bar{Z} \leftarrow \bar{Z} + z_i, \bar{Z}^* \leftarrow \bar{Z}^* + \hat{z}_i^{*,H}$
if $i = n$ **then**
 $\Theta_{t+1} \leftarrow \text{MVEE}\left(\left\{\theta \in \Theta_t : \left(\theta - \underline{W}_t\right)^T \cdot \left(\frac{\bar{Z}^*}{n} - \frac{\bar{Z}}{n}\right) \geq 0\right\}\right)$
 $i \leftarrow 0, \bar{Z} \leftarrow 0, \bar{Z}^* \leftarrow 0$
end if
end if
end for

D.1 Proof of Theorem 3

Proof of Theorem 3. We prove the theorem by showing that the volume of the ellipsoids Θ_t for $t = 1, 2, \dots$ is bounded from below. In conjunction with Lemma 1, which claims there is a minimal

²MDA also works with near optimal experts due to the robustness of MDA. The analysis of this case is identical to the analysis of biased trajectories, as we discuss in the end of Section 2.

rate of decay in the ellipsoid volume, this shows that the number of times the Ellipsoid is updated is polynomially bounded.

We begin by showing that \underline{W}^* always remains in the ellipsoid. We note that in rounds where $V_{c_t}^* - V_{c_t}^{\hat{\pi}_t} > \epsilon$, we have $\underline{W}^{*T} \left(c_t \odot (\mu_{c_t}^* - \mu_{c_t}^{\hat{\pi}_t}) \right) > \epsilon$. In addition, as the agent acts optimally w.r.t. the reward $r_t = c_t^T W_t$, we have that $\underline{W}_t^T \left(c_t \odot (\mu_{c_t}^* - \mu_{c_t}^{\hat{\pi}_t}) \right) \leq 0$. Combining these observations yields:

$$(\underline{W}^* - \underline{W}_t)^T \cdot \left(c_t \odot (\mu_{c_t}^* - \mu_{c_t}^{\hat{\pi}_t}) \right) > \epsilon > 0. \quad (12)$$

This shows that \underline{W}^* is never disqualified when updating Θ_t . Since $\underline{W}^* \in \Theta_0$ this implies that $\forall t : \underline{W}^* \in \Theta_t$. Now we show that not only \underline{W}^* remains in the ellipsoid, but also a small ball surrounding it. If θ is disqualified by the algorithm: $(\theta - \underline{W}_t)^T \cdot \left(c_t \odot (\mu_{c_t}^* - \mu_{c_t}^{\hat{\pi}_t}) \right) < 0$.

Multiplying this inequality by -1 and adding it to (12) yields: $(\underline{W}^* - \theta)^T \cdot \left(c_t \odot (\mu_{c_t}^* - \mu_{c_t}^{\hat{\pi}_t}) \right) > \epsilon$. We apply Hölder inequality to LHS:

$$\begin{aligned} \epsilon &< \text{LHS} \\ &\leq \|\underline{W}^* - \theta\|_\infty \cdot \left\| c_t \odot (\mu_{c_t}^* - \mu_{c_t}^{\hat{\pi}_t}) \right\|_1 \\ &\leq \frac{2k}{1-\gamma} \|\underline{W}^* - \theta\|_\infty \end{aligned}$$

Therefore for any disqualified θ : $\|\underline{W}^* - \theta\|_\infty > \frac{(1-\gamma)\epsilon}{2k}$, thus $B_\infty \left(\underline{W}^*, \frac{(1-\gamma)\epsilon}{2k} \right)$ is never disqualified. This implies that:

$$\forall t : \text{vol}(\Theta_t) \geq \text{vol}(\Theta_0 \cap B_\infty(\underline{W}^*, \frac{(1-\gamma)\epsilon}{2k})) \geq \text{vol}(B_\infty(\underline{W}^*, \frac{(1-\gamma)\epsilon}{4k})).$$

Finally, let M_T be the number of rounds by T in which $V_{c_t}^* - V_{c_t}^{\hat{\pi}_t} > \epsilon$. Using Lemma 1 we get that:

$$\begin{aligned} \frac{M_T}{2(dk+1)} &\leq \log(\text{vol}(\Theta_1)) - \log(\text{vol}(\Theta_{T+1})) \\ &\leq \log(\text{vol}(\text{MVEE}(B_\infty(0, 1)))) - \log(\text{vol}(B_\infty(0, \frac{(1-\gamma)\epsilon}{4k}))) \\ &\leq \log(\text{vol}(\text{MVEE}(B_2(0, \sqrt{dk})))) - \log(\text{vol}(B_2(0, \frac{(1-\gamma)\epsilon}{4k}))) \\ &\leq \log\left(\left(\frac{4k\sqrt{dk}}{(1-\gamma)\epsilon}\right)^{dk}\right) \\ &\leq dk \log \frac{4k\sqrt{dk}}{(1-\gamma)\epsilon}. \end{aligned}$$

Therefore $M_T \leq 2dk(dk+1) \log \frac{4k\sqrt{dk}}{(1-\gamma)\epsilon} = \mathcal{O}(d^2 k^2 \log(\frac{dk}{(1-\gamma)\epsilon}))$. \square

D.2 Proof of Theorem 4

Lemma 2 (Azuma's inequality). *For a martingale $\{S_i\}_{i=0}^n$, if $|S_i - S_{i-1}| \leq b$ a.s. for $i = 1, \dots, n$: $P\left(|S_n - S_0| > b\sqrt{2n \log(\frac{2}{\delta})}\right) < \delta$*

Proof of Theorem 4. We first note that we may assume that for any t : $\|\underline{W}^* - \underline{W}_t\|_\infty \leq 2$. If $\underline{W}_t \notin \Theta_0$, we update the ellipsoid by $\Theta_t \leftarrow \text{MVEE}\left(\left\{\theta \in \Theta_t : \left(\theta - \underline{W}_t\right)^T \cdot e_j \leq 0\right\}\right)$ where e_j is the indicator vector of coordinate j in which \underline{W}_t exceeds 1, and the inequality direction depends on the sign of $(\underline{W}_t)_j$. If $\underline{W}_t \notin \Theta_0$ still, this process can be repeated for a finite number of steps

until $\underline{W}_t \in \Theta_0$, as the volume of the ellipsoid is bounded from below and each update reduces the volume (Lemma 1). Now we have $\underline{W}_t \in \Theta_0$, implying $\|W^* - W_t\|_\infty \leq 2$. As no points of Θ_0 are removed this way, this does not affect the correctness of the proof. Similarly, we may assume $\|W_t^* - W_t\|_\infty \leq 2$ as $W_t^* \in \Theta_0$.

We denote W_t which remains constant for each update in the batch by W . We define $t(i)$ the time-steps corresponding to the demonstrations in the batch for $i = 1, \dots, n$. We define $z_i^{*,H}$ to be the expected value of $\hat{z}_i^{*,H}$, and z_i^* to be the outer product of $c_{t(i)}$ and the feature expectations of the expert policy for $W_{t(i)}^*, c_{t(i)}, \xi'_{t(i)}$. We also denote $W_{t(i)}^*$ by W_i^* . We bound the following term from below, as in Theorem 3:

$$\begin{aligned}
& (\underline{W}^* - \underline{W})^T \cdot \left(\frac{\bar{Z}^*}{n} - \frac{\bar{Z}}{n} \right) \\
&= \frac{1}{n} \sum_{i=1}^n (\underline{W}^* - \underline{W})^T \cdot (\hat{z}_i^{*,H} - z_i) \\
&= \frac{1}{n} \sum_{i=1}^n (\underline{W}^* - \underline{W})^T \cdot (z_i^* - z_i) + \frac{1}{n} \sum_{i=1}^n (\underline{W}^* - \underline{W})^T \cdot (z_i^{*,H} - z_i^*) + \\
&\quad \frac{1}{n} \sum_{i=1}^n (\underline{W}^* - \underline{W})^T \cdot (\hat{z}_i^{*,H} - z_i^{*,H}) \\
&= \underbrace{\frac{1}{n} \sum_{i=1}^n (\underline{W}_i^* - \underline{W})^T \cdot (z_i^* - z_i)}_{(1)} + \underbrace{\frac{1}{n} \sum_{i=1}^n (\underline{W}^* - \underline{W}_i^*)^T \cdot (z_i^* - z_i)}_{(2)} + \\
&\quad \underbrace{\frac{1}{n} \sum_{i=1}^n (\underline{W}^* - \underline{W})^T \cdot (z_i^{*,H} - z_i^*)}_{(3)} + \underbrace{\frac{1}{n} \sum_{i=1}^n (\underline{W}^* - \underline{W})^T \cdot (\hat{z}_i^{*,H} - z_i^{*,H})}_{(4)}
\end{aligned}$$

(1): Since the sub-optimality criterion implies a difference in value of at least ϵ for the initial distribution which assigns 1 to the state where the agent errs, we may use identical arguments to the previous proof. Therefore, the term is bounded from below by ϵ .

(2): By assumption $\|\underline{W}^* - \underline{W}_i^*\|_\infty \leq \frac{(1-\gamma)\epsilon}{8k}$ thus since $\|(z_i^* - z_i)\|_1 \leq \frac{2k}{1-\gamma}$ by Hölder's inequality the term is bounded by $\frac{\epsilon}{4}$.

(3): We have $\|x_i^{*,H} - x_i^*\|_1 \leq \frac{k\gamma^H}{1-\gamma}$ from definitions, thus $\|z_i^{*,H} - z_i^*\|_1 \leq \frac{k\gamma^H}{1-\gamma}$ since $c \in \Delta_{d-1}$. As mentioned previously we may assume $\|W^* - W_t\|_\infty \leq 2$, therefore by Hölder's inequality the term is bounded by $\frac{\epsilon}{4}$ due to our choice of H :

$$\begin{aligned}
\gamma^H &= (1 - (1 - \gamma))^H \\
&= ((1 - (1 - \gamma))^{\frac{1}{1-\gamma}})^{(1-\gamma)H} \\
&= ((1 - (1 - \gamma))^{\frac{1}{1-\gamma}})^{\log(\frac{8k}{(1-\gamma)\epsilon})} \\
&\leq e^{-\log(\frac{8k}{(1-\gamma)\epsilon})} \\
&= \frac{(1 - \gamma)\epsilon}{8k}.
\end{aligned}$$

(4): The partial sums $\sum_{i=1}^N (\underline{W}^* - \underline{W})^T \cdot (z_i^{*,H} - \hat{z}_i^{*,H})$ for $N = 0, \dots, n$ form a martingale sequence. Note that:

$$\|z_i^{*,H}\|_1 \leq \frac{k}{1-\gamma}, \quad \|\hat{z}_i^{*,H}\|_1 \leq \frac{k}{1-\gamma}, \quad \|W^* - W_t\|_\infty \leq 2,$$

thus, we can apply Azuma's inequality (Lemma 2) with $b = \frac{4k}{(1-\gamma)}$ and with our chosen n this yields:

$$\sum_{i=1}^n (\underline{W}^* - \underline{W})^T \cdot (z_i^{*,H} - \hat{z}_i^{*,H}) \leq \frac{n\epsilon}{4} \text{ with probability of at least } 1 - \frac{\delta}{2dk(dk+1) \log(\frac{16k\sqrt{dk}}{(1-\gamma)\epsilon})}.$$

Thus $(\underline{W}^* - \underline{W})^T \cdot (\frac{\bar{Z}^*}{n} - \frac{\bar{Z}}{n}) > \frac{\epsilon}{4}$ and as in Theorem 3 this shows $B_\infty(\underline{W}^*, \frac{(1-\gamma)\epsilon}{8k})$ is never disqualified, and the number of updates is bounded by $2dk(dk + 1) \log(\frac{16k\sqrt{dk}}{(1-\gamma)\epsilon})$, and multiplied by n this yields the upper bound on the number of rounds in which a sub-optimal action is chosen. By union-bound, the required bound for term (4) holds in all updates with probability of at least $1 - \delta$. \square

E Experiments

In this section, we describe the technical details of our experiments, including the hyper-parameters used. To solve MDPs, we use value iteration. Our implementation is based on a stopping condition with a tolerance threshold, τ , such that the algorithm stops if $|V_t - V_{t-1}| < \tau$. In the autonomous driving simulation and grid world domains we use $\tau = 10^{-4}$ and in the dynamic treatment regime we use $\tau = 10^{-3}$.

E.1 Grid world

The grid world domain is an n by m grid which makes $|\mathcal{S}| = n \cdot m$ states. The actions are $\mathcal{A} = \{left, up, right, down\}$ and the dynamics are deterministic for each action, i.e., if the action taken is up, the next state will be the state above the current state in the grid (with cyclic transitions on the borders, i.e., taking the action *right* at state $(n-1, y)$ will transition to $(0, y)$). The features are one-hot vectors ($\phi(s_i) = e_i \in \mathbb{R}^{n \cdot m}$). The contexts correspond to “preferences” of certain states on the grid. The contexts are sampled from a uniform distribution over the $n \cdot m$ dimensional simplex.

This domain is used to evaluate the application of IRL to COIRL problems. We compare the performance of PSGD (COIRL) and the projection algorithm (AL) of Abbeel & Ng (2004) as a function of the context space size. This framework is applied on a grid with dimensions of $3 \cdot 4$, overall 12 states. The PSGD method trains on a CMDP model and the projection algorithm trains on a large MDP model, with a state space that includes the contexts, as noted in Section 2.1. The new states are $s' = (s, c)$, and the new features are $\phi(s') = c \odot \phi(s)$. We measure the run-time of every iteration. The most time-consuming part of both methods is the optimal policy computation time for a given reward. Both methods use the same implementation of value iteration in order to enable a comparison of the run-time. The test data includes 100 contexts.

The results shown in Fig. 7(a) present the value as a function of run-time for each context space size $|\mathcal{C}|$. In Fig. 7(b) we show the accuracy w.r.t. the expert policy in the same manner. We observe that COIRL achieves better value for any size of the train data and that AL achieves better accuracy after convergence. The accuracy over run-time show that the convergence of AL in a large context space takes more time and that the accuracy gap between the methods after convergence is reduced.

E.2 Autonomous driving simulation

The environment is modeled as a tabular MDP that consists of 1531 states. The speed is selected once, at the initial state, and is kept constant afterward. The other 1530 states are generated by 17 X-axis positions for the agent’s car, 3 available speed values, 3 lanes and 10 Y-axis positions in which car B may reside. During the simulation, the agent controls the steering direction of the car, moving left or right, i.e., two actions. The feature vector $\phi(s)$ is composed of 3 features: (1) speed, (2) “collision”, which is set to 0 in case of a collision and 0.5 otherwise, and (3) “off-road”, which is 0.5 if the car is on the road and 0 otherwise.

In these experiments, we define our mappings in a way that induces different behaviors for different contexts, making generalization a more challenging task. We evaluate all algorithms on the same sequences of contexts, and average the results over 5 such sequences. The test data in this domain contains 80 unobserved contexts.

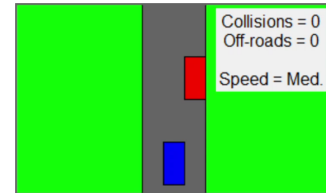
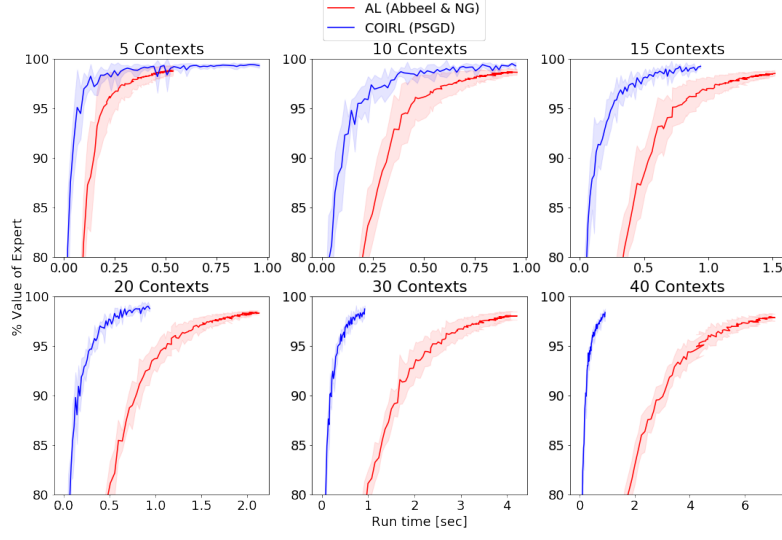


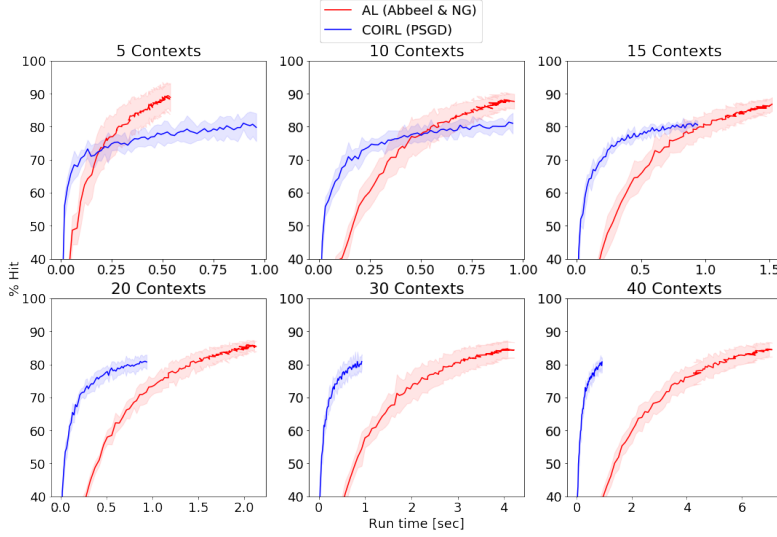
Figure 8: An illustration of the driving simulator.

Ellipsoid setting

The ellipsoid method requires its own framework. Here, the agent’s policy is evaluated by an expert for every new context revealed. Only if its value is not ϵ -close to the optimal policy value, an expert demonstration will be provided (feature expectations of an expert for the revealed context). While the ellipsoid method can only perform a single update for each demonstration, the descent methods can utilize all of the previously revealed demonstrations and perform update steps until convergence.



(a) Value



(b) Accuracy

Figure 7: **value and accuracy as a function of run-time in various context space size.** The advantage of COIRL grows as the context space grows. The plots of COIRL appear to be truncated, that is because the run-time is fixed for any context-space size, in contrast to AL run-time.

The real mapping between the context to the reward is **linear**. We define $W^* = \begin{pmatrix} -1 & 0.75 & 0.75 \\ 0.5 & -1 & 1 \\ 0.75 & 1 & -0.75 \end{pmatrix}$, before normalization. The contexts are sampled uniformly in the 2-dimensional simplex.

Hyper-parameter selection and adjustments: The algorithms maintained a 3×3 matrix to estimate W^* .

Ellipsoid: By definition, the ellipsoid algorithm is hyper-parameter free and does not require tuning.

PSGD: The algorithm was executed with the parameters: $\alpha_0 = 0.3$, $\alpha_t = 0.9^t \alpha_{t-1}$, and iterated for 40 epochs. An outer decay on the step size was added for faster convergence, the initial α_0 becomes $0.94 \cdot \alpha_0$ every time a demonstration is presented. The gradient, g_t is normalized to be $g_t = g_t \frac{g_t}{\|g_t\|_\infty}$ and the calculated step is taken if: $cW_t(\mu(\hat{\pi}_c^t) - \mu(\pi_c^*)) > cW_{t+1}(\mu(\hat{\pi}_c^{t+1}) - \mu(\pi_c^*))$, where $\hat{\pi}_c^t$ denotes the optimal policy for a context c according to W_t .

ES: The algorithm was executed with the parameters: $\sigma = 10^{-3}$, $m = 250$, $\alpha = 0.1$ with decay rate of 0.95, for 50 iterations which didn't iterate randomly over one the contexts, but rather used the entire training set (all of the observed contexts and expert demonstrations up to the current time-step) for each step. The matrix was normalized according to $\|\cdot\|_2$, and so was the step calculated by the ES algorithm, before it was multiplied by α and applied.

Online setting

This section describes the experiment of the online setting. All of the compared methods minimize the same objective, where the subgradients for the descent direction are computed using the feature expectations of the experts. In this framework at every iteration we sample one context and its corresponding feature expectations, and take one descent step according to it. The mapping from context to reward W is linear, and projected to the EW algorithm requirement to be in the $dk - 1$ simplex. In the autonomous driving simulation: $W^* = \begin{pmatrix} 0.043 & 0 & 0.043 \\ 0 & 0.434 & 0 \\ 0.043 & 0.434 & 0 \end{pmatrix}$.

Hyper-parameter selection and adjustments: The PSGD and EW algorithms are configured as the theory specifies, where each descent step is calculated from the one sample. The ES algorithm is applied with the parameters $\sigma = 10^{-3}$, $m = 500$, $\alpha = 0.1$ with decay rate 0.95, for every iteration. The ES implementation include a special enhancement; a descent step is taken if the objective function value decreases (after the descent step).

E.3 Sepsis treatment

For the sepsis treatment we construct two environments, one for simulation purposes - simulator, and another for evaluation on real-life data.

Sepsis treatment simulator

We use the processed data from Jeter et al. (2019). It consists of 5366 trajectories, each representing the sequential treatment provided by a clinician to a patient. At each time-step, the available information for each patient consists of 8 static measurements and 41 dynamic measurements. In addition, each trajectory contains the reported actions performed by the clinician (the number of fluids and vasopressors given to a patient at each time-step and binned to 25 different values), and there is a mortality signal which indicates whether the patient was alive 90 days after his hospital admission.

In order to create a tabular CMDP from the processed data, we separate the static measurements of each patient and keep them as the context. We cluster the dynamic measurements using K-means (MacQueen et al., 1967). Each cluster is considered a state and the coordinates of the cluster centroids are taken as its features $\phi(s)$. We construct the transition kernel between the clusters using the empirical transitions in the data given the state and the performed actions. Two states are added to the MDP and the feature vector is extended by 1 element, corresponding to whether or not the patient died within the 90 days following hospital release. This added feature receives a value of 0 on all non-terminal states, a value of -0.5 for the state representing the patient's death and 0.5 for the one representing survival. In addition, as the number of trajectories is limited, not all state-action pairs are represented in the data. In order to ensure the agent does not attempt to perform an action for which the outcome is unknown, we add an additional terminal state. At this state, all features are set to -1 to make it clearly distinguishable from all other states in the CMDP.

In our simulator, we used the same structure as the raw data, i.e., we used the same contexts found in the data and the same initial state distribution. Each context is projected onto the simplex and the expert's feature expectations for each context are attained by solving the CMDP. While we focus on a simulator, as it allows us to analyze the performance of the algorithms, our goal is to have a reward structure which is influenced by the data. Hence, we produce W^* by running the ellipsoid algorithm on trajectories obtained from the data. As done in the autonomous driving simulation, we average our results over 5 different seeds. The test data size in this domain is 300.

Online setting

There are two setups, In the first one we use the feature expectations of the experts and in the second we use the feature expectations of finite expert trajectories. For the **trajectories** setup we use expert

trajectories of length 40. Again, the mapping from context to reward W is linear, and projected to the EW algorithm requirement to be in the $dk - 1$ simplex (the true mapping can be found in the supplementary code).

Hyper-parameter selection and adjustments: The PSGD method is configured as specified by the theory, where each descent step is calculated from one sample.

Offline setting

The offline setting evaluates the methods' performance on a limited train data set. In this framework, at every iteration we sample a mini-batch of contexts (from a finite set) and their corresponding trajectories (sampled from the expert policy) then taking one descent step according to them. We conduct two experiments that evaluate the performance on a fixed-size data set. First, we consider a **linear** mapping, followed by an analysis of the convergence when a DNN estimator of the reward is used, when the mapping is **non-linear**. Of the various COIRL methods, for these experiments, we focus on PSGD, as it is less restrictive on \mathcal{W} . In all experiments the train data consists of pairs of context and feature expectations of a trajectory of length 40.

We evaluate the PSGD method and (using the mapping calculated by PSGD) along with BC. The evaluation is done after convergence on a changing train data size, measured as 'contexts', which refer to the number of expert trajectories given (one per context). In the non-linear setting, The non-linear model of PSGD implemented by a DNN with the context as its input, three layers with a leakyReLU activation, and batch-normalization, each one of size 336. In both environments, BC is implemented by a DNN that has three layers of sizes: 250,125,25 respectively, a leakyReLU activation between the first and second layers, and a Softmax activation on the output to ensure a probability vector.

Remark 3. *Contextual BC is a method to learn a contextual policy, instead of a contextual reward. In its implementation we use a DNN that, given a context and state-features, computes a probability vector, $\hat{\pi}_c(s)$, representing the agent's policy – i.e., the probability to take action $a \in \mathcal{A}$ is the a 'th element of the DNN output $\hat{\pi}_c(s, a)$. The state-features that are given as an input greatly affect BC performance, especially when we compare it to COIRL, which uses the real dynamics as well as features that represent each state. BC can make good use of the dynamics, as states with similar dynamics should be mapped to similar actions. To improve the performance for BC, we use the same state-features that COIRL uses (HR, blood pressure, etc...), and a feature vector that represents the dynamics. For each state, $s \in \mathcal{S}$, the dynamics can be represented as a concatenation of the probability vectors, $\{P(s, a)\}_{a \in \mathcal{A}}$, where $P(s, a)[i] = P(s, a, s_i)$. The dimension of the dynamics for each state is $|\mathcal{S}| \cdot |\mathcal{A}|$, which is relatively large in the sepsis treatment simulator; hence we reduce its dimensionality with PCA.*

Hyper-parameter selection and adjustments: In the **linear** setting the PSGD algorithm is configured with step-size $\alpha_t = 0.25 \cdot 0.95^t$, the mini-batch size is 10, similarly to the autonomous driving simulation. In this domain the stopping criteria is 60 iterations.

The **non-linear** setting computes the descent direction by backpropagation of the subgradient. Each descent step is calculated over a mini-batch of size 32, where the step-size is $\alpha_t = 0.3 \cdot 0.96^t$. We measure the results for 200 iterations. The train data consists 4000 contexts. The true mapping is defined by $f^*(c) = r_1$ if $\text{age} > 0.1$, and r_2 otherwise, where **age** refers to the normalized age of the patient, an element of the context vector.

E.4 Sepsis treatment in real-world

The sepsis treatment in real-world is described thoroughly in the main paper. Here we describe the evaluation method for the CMDP model and the choice of hyper-parameters, as well as the adjustments that were done to fit the methods to this domain.

Model evaluation: As in The experiments section, we fit a model to the sepsis treatment domain by clustering the patients dynamic measurements. Here we describe the evaluation methods we use to choose the model. Each model is evaluated by two terms: (1) number of different actions taken on the same state for the same patient: $\mathbb{E}_\tau [\mathbb{E}_{s \in \tau} [|\hat{\mathcal{A}}_s^\tau|]]$, where $\hat{\mathcal{A}}_s^\tau = \{a \in \mathcal{A} : (s, a) \in \tau\}$. (2) number of different states in each trajectory: $\mathbb{E}_\tau [|\hat{\mathcal{S}}^\tau|]$, where $\hat{\mathcal{S}}^\tau = \{s \in \mathcal{S} : s \in \tau\}$. In both terms, τ is a trajectory drawn from the data. We require the first term to be as small as possible, to achieve a consistent experts policies in the CMDP model, the second term required to be large, to force the

resulted model to distinguish between different states in the same patient’s trajectory. Obviously, the model has to be as small as possible to enable generalization. The chosen model consists 5000 states.

While processing the data, we noticed that clinicians’ behavior with respect to some measurements is random. To address this matter we consulted with clinicians and defined a set of important dynamic measurements. We then use a clustering process to choose the patients relevant dynamic measurements for the states. States were clustered for any possible single measurement, and the five best dynamic measurements were chosen: mean blood pressure, diastolic blood pressure, shock index, cumulative balance of fluids and the fluids given to a patient. The features in this CMDP are action-dependent and set to be a concatenation of $e_i \in \mathbb{R}^{|S|}$ and $e_j \in \mathbb{R}^{|A|}$ where e_i is a vector of all zeros and a single 1 that represents each state and e_j represents the action, overall there are 5,005 features for each state-action pair.

Hyper-parameter selection and adjustments: For COIRL we report results for the *linear* and the *non-linear* mappings. In both setups, we use a discount factor $\gamma = 0.7$ and a mini-batch of size 32. The stopping criteria is set to stop when five consecutive steps do not increase the validation accuracy. To speed up the validation process we sample a subset of 300 patients from the validation partition at the beginning of each seed and use them to validate the model. In the *linear* setup the step size is $\alpha_t = 0.25 \cdot 0.95^t$. The *non-linear* setup use a DNN to learn the mapping $f_W : \mathcal{C} \rightarrow \mathbb{R}^{|S|+|A|} = \mathbb{R}^{5,005} \approx \mathbb{R}^{5K}$, it has four layers with a Leaky ReLU activation and batch-normalization between the first and second layers, and Leaky ReLU activation between the second and third layers, their sizes are 20K,10K,10K,5K respectively. Here, the step size is $\alpha_t = 0.2 \cdot 0.95^t$

For BC we also use a DNN for function approximation, as we found it to work much better than a linear model. We also experimented with different sets of features as inputs. The features that we found to give the best performance were computed in a similar manner to the features that we used for BC in Remark 3, using the dynamics of the estimated CMDP, resulted in 5K features that represent each state. Concretely, the DNN received a concatenation of the context and the features that represent the current state (size of 5,007) and outputs a stochastic policy (softmax over the outputs of the last layer). The network architecture is composed of three linear layers of sizes 625,125,5. A Leaky ReLU activation follows each layer, and a Softmax activation is used on the output. Similar to COIRL, the model is trained over the training set partition, and the stopping criteria are set to stop after five epochs of non-increasing validation accuracy. The loss of the DNN is the binary cross-entropy loss between the DNN output and the observed action, $e_i \in \mathbb{R}^{|A|}$. The mini-batch size is 32 and the optimizer is SGD with step size $\alpha_t = 0.1 \cdot \frac{1}{1+10^{-7}t}$.

E.5 Infrastructure and run-times

We summarize the infrastructure and average run-time for each experiment in Table 3. Note that the run-times correspond with the run-time of all seeds of each experiment, for all methods.

Experiment		Method	Infrastructure	Run-time
Grid world		PSGD	Processor: Intel Core i7-5930K Memory: 68.2 GiB	2 hours
		AL	Graphics: Geforce GTX TITAN X	4 hours
Autonomous driving	Ellipsoid setting	PSGD	AWS EC2 machine	2 days
		ES	# Cores: 96	1 week
		Ellipsoid	Memory: 384 GiB	1-2 days
	Online setting	PSGD	Processor: Intel Core i7-5930K	12 hours
		EW	Memory: 68.2 GiB	12 hours
		ES	Graphics: Geforce GTX TITAN X	3 days
	Sepsis treatment	Online setting	PSGD	Processor: Intel Core i7-5930K
Offline setting		PSGD	Memory: 68.2 GiB	3-4 days
		BC	Graphics: Geforce GTX TITAN X	2-3 days
Sepsis treatment in real-world		PSGD	Processor: Intel Core i7-5930K Memory: 68.2 GiB	1-2 weeks
		BC	Graphics: Geforce GTX TITAN X	1 week

Table 3: Run-times of each experiment and infrastructures used to conduct each experiment. The run-time of PSGD in the sepsis treatment in real-world includes the model fitting process.